Dynamic Networks in Large Financial and Economic Systems

Jozef Baruník[‡] and Michael Ellington[†]
May 28, 2022

Abstract

We propose new measures to characterize dynamic network connections in large financial and economic systems. In doing so, our measures allow one to describe and understand causal network structures that evolve throughout time and over horizons using variance decomposition matrices from time-varying parameter VAR (TVP VAR) models. These methods allow researchers and practitioners to examine network connections over any horizon of interest whilst also being applicable to a wide range of economic and financial data. Our empirical application redefines the meaning of "big" in big data, in the context of TVP VAR models, and track dynamic connections among illiquidity ratios of all S&P500 constituents. We then study the information content of these measures for the market return and real economy.

JEL Classifications: C10, C40, C55, C58, G00

Keywords: Dynamic networks, Network connections, Time-varying parameter VAR, Liquidity

[‡]Institute of Economic Studies, Charles University, Opletalova 26, 110 00, and The Czech Academy of Sciences, IITA, Pod Vodárenskou Věží 4, 182 08, Prague, Czech Republic. barunik@fsv.cuni.cz

[†]University of Liverpool Management School, Chatham Building, Liverpool, L69 7ZH, UK. m.ellington@liverpool.ac.uk

1 Introduction

Economic agents create links among one another. These relationships can be seen through a variety of data such as: the co-movement of economic variables like consumption growth (e.g. Richmond, 2019); financial variables including stock return volatilities (e.g. Herskovic et al., 2020); and firm characteristics describing the supply chain (e.g. Garvey et al., 2015). A natural way to describe and understand these connections is to view them as a network. Viewing linkages in this manner allows one to characterize and track connections through entities of interest, and also contributes to understanding how shocks propagate throughout a system.

However, connections evolve over time and shocks creating network linkages possess differences in persistence. The implication here is that network connections, and shock propagation throughout these systems, are dynamic over time and across horizons. Adding to this, the emergence of big data sources means that the dimensions of network structures that researchers and practitioners wish to understand are growing rapidly. Despite these two issues, dynamic networks remain ill-defined and poorly understood. Researchers and practitioners are bound to thinking in terms of correlation-based measures and methods that permit time-variation into the modelling process either being infeasible or computationally inefficient.

In this paper, we propose dynamic network measures that stem from time-varying parameter VAR (TVP VAR) models. Our measures not only allow users to describe and understand network structures that evolve throughout time and over horizons, but also are readily available in the presence of big data. Adding to this, they have direct causal interpretation that permits the understanding of how shocks with different persistence create dynamic networks among economic and financial variables. Our methods are applicable to a wide range of economic and financial data. We illustrate by characterizing dynamic network connections among illiquidity proxies of N=496 financial assets. We then demonstrate its usefulness in two applications. First we relate dynamic network measures the market return, and then to the real economy and financial stress indicators.

Typically, the network literature in economics and finance study static networks (see e.g. Elliott et al., 2014; Glasserman and Young, 2016). To illustrate this, Figure 1 (a) shows a star topology where variable 1 is central and its shocks propagate to the remaining N variables. In this case, variable 1 is creating a directed, or asymmetric network in which the nodes are connected with the same strength. Figure 1 (b) is an N star network topology where the links among the N central variables have weighted strengths. While

the network is more complex, it is missing key ingredients to be able to describe dynamic network in the economic and financial systems. First, these networks cannot adequately capture evolving relationships among variables. Second, the network describes aggregate connections across different horizons, while short-term, medium-term, and long-term connections are hidden.

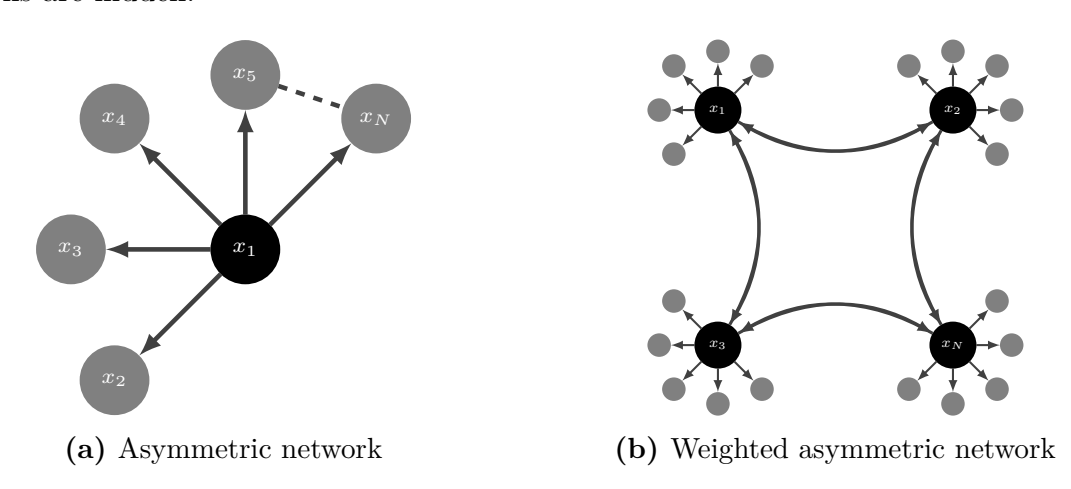


Figure 1: Emergence of Network: The sub-figure (a) presents a network containing x_1, \ldots, x_N variables represented as nodes. Here node x_1 influences all other x_2, \ldots, x_N nodes. Nodes x_2, \ldots, x_N are not connected to each other and also do not influence node x_1 . The sub-figure (b) presents an N-star network where nodes x_1, \ldots, x_N are connected to a set of nodes exclusively, and also to one another. Arrows denote the direction of the connection and the density of the line denotes the strength of the connections.

Our approach provides a potential resolution to the account for the two key ingredients prior work misses. To illustrate, Figure 2 introduces a dynamic network with multiple layers that represent distinct connections among variables. We interpret these links as dynamic horizon specific network connections where the layers distinguish short-term and long-term linkages. Without loss of generality, the curves connecting the N central variables allow for the possibility of connections across layers. We represent time dynamics of network connections at periods $t = 1, \ldots, T$ on a time line.

For simplicity we assume that the N central variables are the same across each layer but will have connections of different strengths over time and horizon. Specifically, network connections are more intense in the long run during the first period relative to the short run meaning that relationships are more persistent and a shock to the central variables will create linkages with a long-run strengths. During the second period long-term network connections lose their strength and network connections are stronger in the short run.

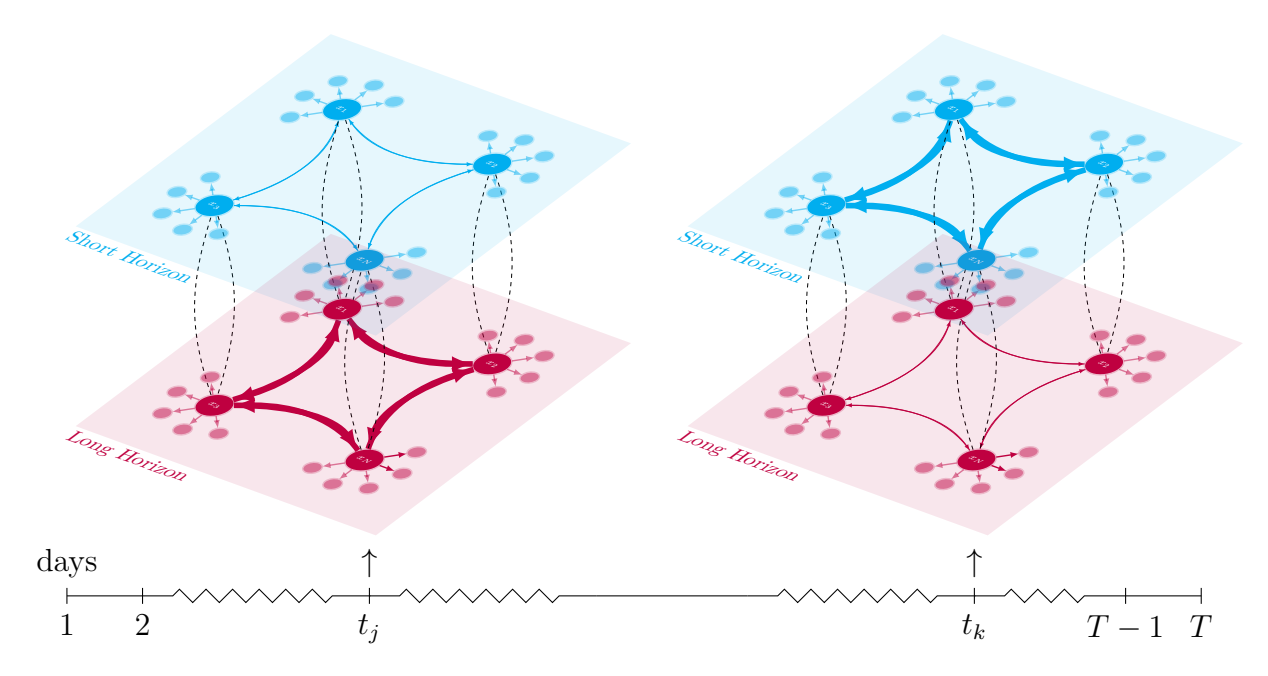


Figure 2: A Dynamic Horizon Specific Network: This figure presents a multi-layer N-star network with snapshot of two time and two horizon specific network layers. Arrows denote directions of connections and the line density denotes strength. The curves from the N central nodes allow for connections to spillover across layers. We interpret each layer as a network specific to a horizon of interest; for example short-term depicted by light blue color and long-term depicted by light red color.

Our main objective is to provide a framework for tracking and understanding the causal nature of dynamic networks that form within a potentially large system of variables. Current studies almost exclusively examine static networks that mimic time dynamics using an approximating window (see e.g. Demirer et al., 2018)¹. In doing so, we employ a locally stationary TVP VAR that allows us to estimate the adjacency matrix for a network at each point in time using the variance decomposition matrix. We decompose this into horizon specific components that allow us to disentangle short-term, medium-term, and long-term network connections. Our methods are general enough to permit one to examine any horizon of interest, such as over the business cycle for macroeconomic applications, or even on a daily basis for financial applications.

Variance decompositions are a natural way to characterize a network working with causal linkages. Specifically, variance decompositions tell us much of the future variance of variable j is due to shocks in variable k, and under mild assumptions have a direct causal interpretation (Rambachan and Shephard, 2019). The variance decomposition matrix

¹Geraci and Gnabo (2018) estimates multiple pairwise time varying parameter models in an attempt to characterize a network of financial stocks using autoregressive coefficients.

defines the network adjacency matrix completely. It is intimately related to network node degrees, mean degrees, and connectedness measures (Diebold and Yilmaz, 2014). We label our network structures as dynamic horizon specific networks that stem from time-varying variance decompositions.

Our network structures build on classical network structures. In a typical network, the adjacency matrix contains zero and one entries, depending on the node being linked or not, respectively. In the above notion, one interprets variance decompositions as weighted links showing the strength of the connections. In addition, the links are directed, meaning that the j to k link is not necessarily the same as the k to j link, and hence, the adjacency matrix is not symmetric. Therefore we can define weighted, directed versions of network connectedness statistics readily that include degrees, degree distributions, distances and diameters.

We consider horizon specific dynamics of network connections by using the spectral representation of the variance decomposition matrix. A shock with a strong long-term effect will have high power at low frequencies, and in case it transmits to other variables, it creates long-term connectedness. Long-term connectedness of economic variables may be attributable to permanent changes in expectations of economic agents. Conversely, short-term connections may appear when changes are transitory. Baruník and Křehlík (2018) define notion of the horizon specific connectedness measures for a simple VAR that we further generalize to a locally stationary processes here. To capture horizon-specific dynamic network connections, we propose a general framework for decomposing the aggregate dynamic network to any frequency, or horizon specific, band of interest.

Our empirical applications show the usefulness of dynamic network connections that form on individual stock illiquidities for the market return, and the real economy². Regarding the former, we uncover a strong link between the market return and illiquidity network connections that intensifies during periods of financial stress. We link this to the reinforcing mechanism between market and funding liquidity in Brunnermeier and Pedersen (2009) and argue that our measures may be of use for portfolio formation and/or rebalancing. Concerning the latter, we document a negative (positive) link with real activity (financial stress indicators). We relate this finding to Kiyotaki and Moore (2019) and suggest that our illiquidity connectedness measures act as indices that track horizon

²There is a growing literature that focuses on illiquidity. For example some focus on the pricing implications of liquidity risk (see e.g. Pástor and Stambaugh (2003), Acharya and Pedersen (2005), Bekaert et al. (2007)). Meanwhile others concentrate on the dynamics of market illiquidity and market returns (Amihud, 2002; Chen et al., 2018); as well as the link between market illiquidity and the real economy (Næs et al., 2011; Ellington, 2018)

specific systemic shock propagation.

The remainder of this paper proceeds as follows. Section 2 describes our methodology in tracking dynamic horizon specific network connections. In Section 3, we discuss data and how we track horizon specific dynamic illiquidity network connections for a system containing all S&P500 constituents. Our empirical results relating network connectedness to the dynamics of market returns and showing its usefulness for the real economy and financial stress indicators are in Section 4. Finally, conclusion are given in Section 5.

2 Measurement of Dynamic Causal Network Connectedness

Our measures rely on locally stationary processes because this assumes the process is approximately stationary over a short time interval. Intuitively, this allows us to incorporate time-variation and establish our measures of horizon specific time-varying network connections. Consider a doubly indexed N-variate time series $(X_{t,T})_{1 \le t \le T,T \in \mathbb{N}}$ with components $X_{t,T} = (X_{t,T}^1, \ldots, X_{t,T}^N)^{\top}$ that describe all variables in an economy. Here t refers to a discrete time index and T is an additional index indicating the sharpness of the local approximation of the time series $(X_{t,T})_{1 \le t \le T,T \in \mathbb{N}}$ by a stationary one. Coarsely speaking, we can consider $(X_{t,T})_{1 \le t \le T,T \in \mathbb{N}}$ to be a weakly locally stationary process if, for a large T, given a set S_T of sample indices such that $t/T \approx u$ over $t \in S_T$, the sample $(X_{t,T})_{t \in S_T}$ approximates the sample of a weakly stationary time series depending on the rescaled location u. Note that u is a continuous time parameter referred to as the rescaled time index, and T is interpreted as the number of available observation, hence $1 \le t \le T$ and $u \in [0, 1]$, see Dahlhaus (1996) for further details.

We assume assets to follow a locally stationary TVP-VAR of lag order p as

$$\boldsymbol{X}_{t,T} = \boldsymbol{\Phi}_1(t/T)\boldsymbol{X}_{t-1,T} + \ldots + \boldsymbol{\Phi}_p(t/T)\boldsymbol{X}_{t-p,T} + \boldsymbol{\epsilon}_{t,T}, \tag{1}$$

where $\boldsymbol{\epsilon}_{t,T} = \boldsymbol{\Sigma}^{-1/2}(t/T)\boldsymbol{\eta}_{t,T}$ with $\boldsymbol{\eta}_{t,T} \sim NID(0, \boldsymbol{I}_M)$ and $\boldsymbol{\Phi}(t/T) = (\boldsymbol{\Phi}_1(t/T), \dots, \boldsymbol{\Phi}_p(t/T))^{\top}$ are the time varying autoregressive coefficients. In a neighborhood of a fixed time point $u_0 = t_0/T$, we approximate the process $\boldsymbol{X}_{t,T}$ by a stationary process $\boldsymbol{X}_t(u_0)$ as

$$\widetilde{\boldsymbol{X}}_{t}(u_{0}) = \boldsymbol{\Phi}_{1}(u_{0})\widetilde{\boldsymbol{X}}_{t-1}(u_{0}) + \ldots + \boldsymbol{\Phi}_{p}(u_{0})\widetilde{\boldsymbol{X}}_{t-p}(u_{0}) + \boldsymbol{\epsilon}_{t}, \tag{2}$$

with $t \in \mathbb{Z}$ and under suitable regularity conditions $|X_{t,T} - \widetilde{X}_t(u_0)| = O_p(|t/T - u_0| + 1/T)$

which justifies the notation "locally stationary process." Crucially, the process has time varying $VMA(\infty)$ representation (Dahlhaus et al., 2009; Roueff and Sanchez-Perez, 2016)

$$\boldsymbol{X}_{t,T} = \sum_{h=-\infty}^{\infty} \boldsymbol{\Psi}_{t,T}(h) \boldsymbol{\epsilon}_{t-h}$$
(3)

where $\Psi_{t,T}(h) \approx \Psi(t/T, h)$ is a stochastic process satisfying $\sup_{\ell} ||\Psi_t - \Psi_{\ell}||^2 = O_p(h/t)$ for $1 \leq h \leq t$ as $t \to \infty$. Since $\Psi_{t,T}(h)$ contains an infinite number of lags, we approximate the the moving average coefficients at $h = 1, \ldots, H$ horizons. The connectedness measures rely on variance decompositions, which are transformations of the $\Psi_{t,T}(h)$ and will allow the measurement of the contribution of shocks to the system.

Since a shock to a variable in the model does not necessarily appear alone, i.e. orthogonally to shocks to other variables, an identification scheme is crucial in calculating variance decompositions. We will adapt a generalized identification proposed by Pesaran and Shin (1998) to a locally stationary processes. An important feature of the generalized impulse responses is its direct causal interpretation. Under the mild conditions (Rambachan and Shephard, 2019), our measures will be causal measures.

Moreover, as argued by Baruník and Křehlík (2018) a natural way to describe horizon specific dynamics (the long-term, medium-term, or short-term) of the connectedness in the network is to consider a spectral representation of the approximating model. Hence instead of impulse responses in the system, we will focus on the frequency response of a shock that in addition will be local. As a building block of the measures, we consider a time-varying frequency response function $\Psi_{t/T}e^{-i\omega} = \sum_h e^{-i\omega h}\Psi_{t,T}(h)$ which we obtain from a Fourier transform of the coefficients with $i = \sqrt{-1}$.

A unique time varying spectral density of $X_{t,T}$ at frequency ω which is locally the same as the spectral density of $\widetilde{X}_t(u)$ at u = t/T can be defined as a Fourier transform of VMA(∞) filtered series as

$$S_{X}(u,\omega) = \sum_{h=-\infty}^{\infty} \mathbb{E}\left[\widetilde{X}_{t+h}(u)\widetilde{X}_{t}^{\top}(u)\right] e^{-i\omega h} = \left\{\Psi(u)e^{-i\omega}\right\} \Sigma(u) \left\{\Psi(u)e^{+i\omega}\right\}^{\top}.$$
(4)

The time-varying spectral density is a key quantity for understanding frequency dynamics, since it describes how the variance of the time varying covariance of $X_{t,T}$ is distributed over the frequency components ω . Using the spectral representation for the local covariance that is associated with local spectral density,

$$\mathbb{E}\left[\widetilde{\boldsymbol{X}}_{t+h}(u)\widetilde{\boldsymbol{X}}_{t}^{\top}(u)\right] = \int_{-\pi}^{\pi} \boldsymbol{S}_{\boldsymbol{X}}(u,\omega)e^{i\omega h}d\omega \tag{5}$$

we can naturally introduce time varying frequency domain counterparts of variance decompositions.

The following proposition³ establishes time varying spectral representation of the variance decomposition of shocks from asset j to asset k, and it is central to the development of the network connectedness measures in the time-frequency domain.

Proposition 1 (Dynamic Adjacency Matrix). Suppose $X_{t,T}$ is a weakly locally stationary process with

$$\sigma_{kk}^{-1} \sum_{h=0}^{\infty} \left| \left[\Psi(u, h) \Sigma(u) \right]_{j,k} \right| < +\infty, \forall j, k.$$

Then the **time-frequency variance decompositions** of the jth variable at a rescaled time $u = t_0/T$ due to shocks in the kth variable on the frequency band $d = (a, b) : a, b \in (-\pi, \pi), a < b$ forming a **dynamic adjacency matrix** is defined as

$$\left[\boldsymbol{\theta}(u,d)\right]_{j,k} = \frac{\sigma_{kk}^{-1} \int_{a}^{b} \left| \left[\boldsymbol{\Psi}(u)e^{-i\omega}\boldsymbol{\Sigma}(u)\right]_{j,k} \right|^{2} d\omega}{\int_{-\pi}^{\pi} \left[\left\{\boldsymbol{\Psi}(u)e^{-i\omega}\right\}\boldsymbol{\Sigma}(u)\left\{\boldsymbol{\Psi}(u)e^{+i\omega}\right\}^{\top}\right]_{j,i} d\omega}$$
(6)

where $\Psi(u)e^{-i\omega} = \sum_h e^{-i\omega h}\Psi(u,h)$ is local impulse transfer function or frequency response function computed as the Fourier transform of the local impulse response $\Psi(u,h)$

Proof. See Appendix A.
$$\Box$$

It is important to note that $\left[\boldsymbol{\theta}(u,d)\right]_{j,k}$ is a natural dissagregation of traditional variance decompositions to time-varying frequency bands, since portion of the local error variance of the jth variable at a given frequency band due to shocks in the kth variable is scaled by the variance of the jth variable. Note that while the Fourier transform of the impulse response is generally a complex valued quantity, the quantity introduced by proposition (1) is the squared modulus of the weighted complex numbers, thus producing a real quantity.

This relationship is an identity which means the integral is a linear operator, summing over disjoint intervals covering the entire range $(-\pi, \pi)$ recovers the time domain counterpart of the local variance decomposition. The following remark formalizes this fact.

³Note to notation: $[A]_{j,k}$ denotes the jth row and kth column of matrix A denoted in bold. $[A]_{j,k}$ denotes the full jth row; this is similar for the columns. A $\sum A$, where A is a matrix that denotes the sum of all elements of the matrix A.

Remark 1 (Aggregation of Adjacency Matrix). Denote by d_s an interval on the real line from the set of intervals D that form a partition of the interval $(-\pi, \pi)$, such that $\bigcap_{d_s \in D} d_s = \emptyset$, and $\bigcup_{d_s \in D} d_s = (-\pi, \pi)$. Due to the linearity of integral and the construction of d_s , we have

$$\left[\boldsymbol{\theta}(u,\infty)\right]_{j,k} = \sum_{d_s \in D} \left[\boldsymbol{\theta}(u,d_s)\right]_{j,k}.$$

Remark (1) is important as it establishes the aggregation of frequency specific network connectedness measures to its time domain, *total* counterpart. Hence one can easily obtain short-term, medium-term, and long-term time varying network connectedness characteristics that will always sum up to an aggregate time domain counterpart.

As the rows of the time-frequency network connectedness do not necessarily sum to one, we normalize the element in each by the corresponding row sum

$$\left[\widetilde{\boldsymbol{\theta}}(u,d)\right]_{j,k} = \left[\boldsymbol{\theta}(u,d)\right]_{j,k} / \sum_{k=1}^{N} \left[\boldsymbol{\theta}(u,\infty)\right]_{j,k}$$
 (7)

Our notion that we can approximate well the process $X_{t,T}$, by a stationary process $\widetilde{X}_t(u)$ in a neighborhood of a fixed time point u = t/T, means that all associated local quantities approximate well their time varying counterparts. Following the arguments in Dahlhaus (1996) and using mild assumptions one can easily see that local variance decompositions at a frequency band $\widetilde{\theta}(u,d)$ approximate well the time-varying variance decompositions of the process $X_{t,T}$.

Note that local generalized variance decompositions form a dynamic network adjacency matrix defining a time-varying network at a given frequency band. Hence we can use these measures directly as a time-varying network connectedness that contains richer information in comparison to typical network analysis. In a typical network, adjacency matrix is filled with zero and one entries depending on the node being linked or not. In our notion, variance decompositions can be viewed as weighted links showing strengths of the connections. In addition, the links are directional, meaning that the j to k link is not necessarily the same as the k to j link, and hence the adjacency matrix is asymmetric. Even more important, using our notion above, the adjacency matrix is time-varying and frequency specific that allows the study of time-varying network connectedness at various frequency bands of the user's choice.

Now we can define network connectedness measures that characterize a time varying horizon specific network. We define local network connectedness measures at a given frequency band as the ratio of the off-diagonal elements to the sum of the entire matrix

$$C(u,d) = 100 \times \sum_{\substack{j,k=1\\j \neq k}}^{N} \left[\widetilde{\boldsymbol{\theta}}(u,d) \right]_{j,k} / \sum_{j,k=1}^{N} \left[\widetilde{\boldsymbol{\theta}}(u,\infty) \right]_{j,k}$$
 (8)

This measures the contribution of forecast error variance attributable to all shocks in the system, minus the contribution of own shocks. Similar to the local network aggregate connectedness measure that infers the system-wide connectedness, we can define measures that will reveal when an individual variable in the economy is transmitter or receiver of shocks. The local directional connectedness that measures how much of each variables's j variance is due to shocks in other variable $j \neq k$ in the economy is given by

$$C_{j \leftarrow \bullet}(u, d) = 100 \times \sum_{\substack{k=1\\k \neq j}}^{N} \left[\widetilde{\boldsymbol{\theta}}(u, d) \right]_{j, k} / \sum_{j, k=1}^{N} \left[\widetilde{\boldsymbol{\theta}}(u, \infty) \right]_{j, k}, \tag{9}$$

defining the so-called FROM connectedness. Note that this quantity can be precisely interpreted as from-degrees (often called out-degrees in the network literature) associated with the nodes of the weighted directed network represented by the variance decompositions matrix generalized to a time-varying frequency specific quantity. Likewise, the contribution of variable j to variances in other variables is computed as

$$C_{j \to \bullet}(u, d) = 100 \times \sum_{\substack{k=1\\k \neq j}}^{N} \left[\widetilde{\boldsymbol{\theta}}(u, d) \right]_{k, j} / \sum_{j, j=1}^{N} \left[\widetilde{\boldsymbol{\theta}}(u, \infty) \right]_{k, j}$$
 (10)

and is the so-called TO connectedness. Again, this can be precisely interpreted as to-degrees (often called in-degrees in the network literature) associated with the nodes of the weighted directed network represented by the variance decompositions matrix. These two measures show how other assets contribute to the risk of asset j, and how asset j contributes to the riskiness of others, respectively, in a time varying fashion at a chosen frequency band.

Proposition 2 (Reconstruction of Dynamic Network Connectedness). Denote by d_s an interval on the real line from the set of intervals D that form a partition of the interval $(-\pi, \pi)$, such that $\cap_{d_s \in D} d_s = \emptyset$, and $\cup_{d_s \in D} d_s = (-\pi, \pi)$. We then have that

$$C(u, \infty) = \sum_{d_s \in D} C(u, d_s)$$

$$C_{j \leftarrow \bullet}(u, \infty) = \sum_{d_s \in D} C_{j \leftarrow \bullet}(u, d_s)$$

$$C_{j \rightarrow \bullet}(u, \infty) = \sum_{d_s \in D} C_{j \rightarrow \bullet}(u, d_s)$$
(11)

where $C(u, \infty)$ are local network connectedness measures aggregated over frequencies with $H \to \infty$.

Proof. See Appendix A.
$$\Box$$

In light of the above, all local frequency connectedness measures C(u, d) for u = t/T approximate well the time-varying frequency connectedness of the process $X_{t,T}$, that is $C_{t,T}(d)$.

Finally, we note that our measures can be have a direct causal interpretation. Rambachan and Shephard (2019) provide a discussion about causal interpretation of impulse response analysis in the time series literature. In particular, they argue that if an observable time series is shown to be a *potential outcome* time series, then generalized impulse response functions have a direct causal interpretation. Potential outcome series describe at time t the output for a particular path of treatments.

In the context of our study, paths of treatments are shocks. The assumptions required for a potential outcome series are natural and intuitive for a typical economic and/or financial time series: i) they depend only on past and current shocks; ii) series are outcomes of shocks; and iii) assignment of shocks depend only on past outcomes and shocks. The dynamic adjacency matrix we introduce in Proposition 1 is a transformation of generalized impulse response functions. Therefore, the dynamic adjacency matrix and all measures that stem from manipulations of its elements possess a causal interpretation; thus establishing the notion of causal dynamic network measures.

2.1 Obtaining horizon specific network risk measures from large dynamic networks

In light of the assumptions that underpin our measures, we conjecture that the economy (or market) follows a stable time-varying parameter heteroskedastic VAR (TVP-VAR) model as in (1). To obtain the time-varying coefficient estimates at a fixed time point

 $u = t_0/T$, $\Phi_1(u), ..., \Phi_p(u)$, and the time-varying covariance matrices, $\Sigma(u)$, we estimate the model using Quasi-Bayesian Local-Liklihood (QBLL) methods (Petrova, 2019).

Specifically, this approach uses a kernel weighting function that provides larger weights to observations that surround the period whose coefficient and covariance matrices are of interest. Using conjugate priors, the (quasi) posterior distribution of the parameters of the model are analytical. This alleviates the need to use a Markov Chain Monte Carlo (MCMC) simulation algorithm and permits the use of parallel computing. Note also that in using (quasi) Bayesian estimation methods, we obtain a distribution of parameters that we use to construct network measures that provide confidence bands. Details of the model and estimation algorithm are in Appendix B.⁴ We provide a computationally efficient package DynamicNets.jl in JULIA and DynamicNets in MATLAB that allows one to obtain our measures on data the researcher desires.⁵

We provide some details on estimation here. First, the variance decompositions of the forecast errors from the VMA(∞) representation require a truncation of the infinite horizon with a H horizon approximation. As $H \to \infty$ the error disappears (Lütkepohl, 2005). We note here that H serves as an approximating factor and has no interpretation in the time-domain. We obtain horizon specific measures using Fourier transforms and set our truncation horizon H=100; results are qualitatively similar for $H \in \{50, 100, 200\}$. Second in computing our measures, we diagonalize the covariance matrix because our objective is to focus on the causal affects of network connections. The $\Psi(u,h)$ matrix embeds the causal nature of network linkages, and the covariance matrix $\Sigma(u)$ contains contemporaneous covariances within the off-diagonal elements. In diagonalizing the covariance matrix we remove the contemporaneous effects and focus solely on causation.

3 Building a dynamic horizon specific network among S&P500 constituent illiquidity measures

To illustrate our methodology, we focus on characterizing network connections among illiquidity proxies of financial assets. However, it is worth noting that our dynamic network measures can be applied to a wide range of economic and financial data. An

⁴Unlike traditional TVP VARs time-variation evolves in a non-parametric manner thus making no assumption on the laws of motion within the model. Typically, the model of Primiceri (2005), and many extensions, assume parameters evolve as random walks or autoregressive processes.

⁵The packages are available at https://github.com/barunik/DynamicNets.jl and https://github.com/ellington/DynamicNets

abundance of work focuses on the pricing implications of liquidity risk (see e.g. Pástor and Stambaugh (2003), Acharya and Pedersen (2005), Bekaert et al. (2007)). However, there are emerging studies concerning the dynamics of market illiquidity and market returns (Amihud, 2002; Chen et al., 2018); as well as the link between illiquidity and the real economy (Næs et al., 2011; Ellington, 2018).

There are various channels through which illiquidity can influence returns and the real economy. First, a liquid stock market permits the ease of trading assets which people rely on to ensure fair pricing. Second, a liquid stock market may reveal the information set of investors. For example if market participants anticipate future declines to liquidity conditions, their adjustments into safer, and more liquid, assets reflect this expectation (Florackis et al., 2014). From a theoretical perspective, Brunnermeier and Pedersen (2009) link funding and market liquidity which creates a mechanism for liquidity to influence returns and the real economy. Specifically, this link intensifies during periods of financial decline which causes mutually reinforcing "liquidity spirals" which puts persistent downward pressure on prices; and therefore depletes returns.

Adding to this, Kiyotaki and Moore (2019) provide a mechanism through which liquidity shocks affect the real economy. In particular, people within this economy sell holdings for liquid assets in order to finance investment opportunities due to binding borrowing constraints. Liquidity in this context refers to resaleability of assets which change due to the order flow. Successive orders change trading costs which in turn changes the ease of reselling assets. When prices become more sensitive to the order flow, the ease of reselling assets falls. In turn, the cost of trading rises, investment deteriorates, which spurs contractions in real activity.

The purpose of our illustration is on how network connections form among illiquidities of individual stocks. We use the result in Acemoglu et al. (2012) that network structures allow idiosyncratic shock propagation throughout a network structure to determine aggregate fluctuations. Chordia et al. (2000) document that liquidity measures, on a country-by-country basis, exhibit a common component; we also see this in the data at an individual stock level.

Naturally, viewing individual stock's liquidity measures as nodes in a network allows one to track and characterize network connections. In our application, we build a dynamic network on a daily basis using all constituents listed on the S&P500 from July 8, 2005 to August 31, 2018. We aggregate high-frequency price and trading volume data from Tick Data. For each of N=496 stocks, we compute their daily returns $R_t = \sum_{i=1}^{D} (p_{t,i} - p_{t,i-1})$ and trading volume VOL_t = $\sum_{i=1}^{D} \text{vol}_{t,i}$ on day t where D denotes the total number of

intraday observations. The subscript i denote intraday observations which we observe at 5 minute intervals; and $p_{t,i}$, $vol_{t,i}$ are the intraday price and trading volume of the asset respectively. We then convert trading volume into \$ trading volume by multiplying by the closing price of the stock on day t. We then compute each stock's Amihud (2002) ratio as

$$ILLIQ_t = \frac{|R_t|}{DVOL_t}$$
 (12)

where $|R_t|$ is the stock's day t absolute daily return, and DVOL_t is the stock's dollar trading volume on day t.

The Amihud (2002) ratio captures the price impact dimension of illiquidity and measures the elasticity of the stock price with respect to a \$1, in our case, change in trading volume. This measure has strong theoretical links with the price impact coefficient in Kyle (1985). This tracks the sensitivity of asset prices to the order flow; empirically, Goyenko et al. (2009) show that the Amihud (2002) ratio is a good proxy for price impact. Furthermore, these price impact ratios link well with the economic mechanism of liquidity shocks in Kiyotaki and Moore (2019).

A feature of a stock's illiquidity is its positive correlation with volatility. This raises the question whether proxies for illiquidity capture illiquidity or effects attributable to volatility. Also, volatility may contain information regarding future prices and the state of the economy that bears no link with illiquidity (Bansal et al., 2014). Following Chen et al. (2018), we orthogonalize each stock's ILLIQ $_t$ measure by taking the residuals of a regression of ILLIQ $_t$ on the corresponding stock's contemporaneous realized volatility measure. Formally for each stock, their volatility-free measure of illiquidity is:

$$ILLIQ_t^{\perp RV} = ILLIQ_t - a - b \times RV_t$$
(13)

where a and b are regression coefficients, and RV_t is the stock's realized volatility measure that we construct as RV_t = $\sqrt{\sum_{i=1}^{D} (p_{t,i} - p_{t,i-1})^2}$ with D denoting the number of intraday observations, and $p_{t,i}$ is the intraday stock price.

We estimate the TVP VAR as in (1) on N=496 stock's volatility-free illiquidity measures with p=2 lags on our T=3275 days of data. We estimate dynamic horizon specific network measures on a 48-core server and for every time period we generate 500 simulations of the quasi-posterior distribution; this results in a total estimation time of 10 days.

We compute dynamic network measures at short-, medium-, and long-term horizons. Short-term captures connections at horizons 1-day to 1-week; medium-term captures connections at horizons 1-week to 1-month; and long-term captures at horizons greater than 1-month. Figure 3 shows total dynamic network connectedness, we define $C_{t,T}^d$, $d = \{S, M, L\}$ over the short-term, S; medium-term, M; and long-term, L as an approximation for the theoretical quantity C(u, d) such that $C_{t,T}^d \approx C(u, d)$.

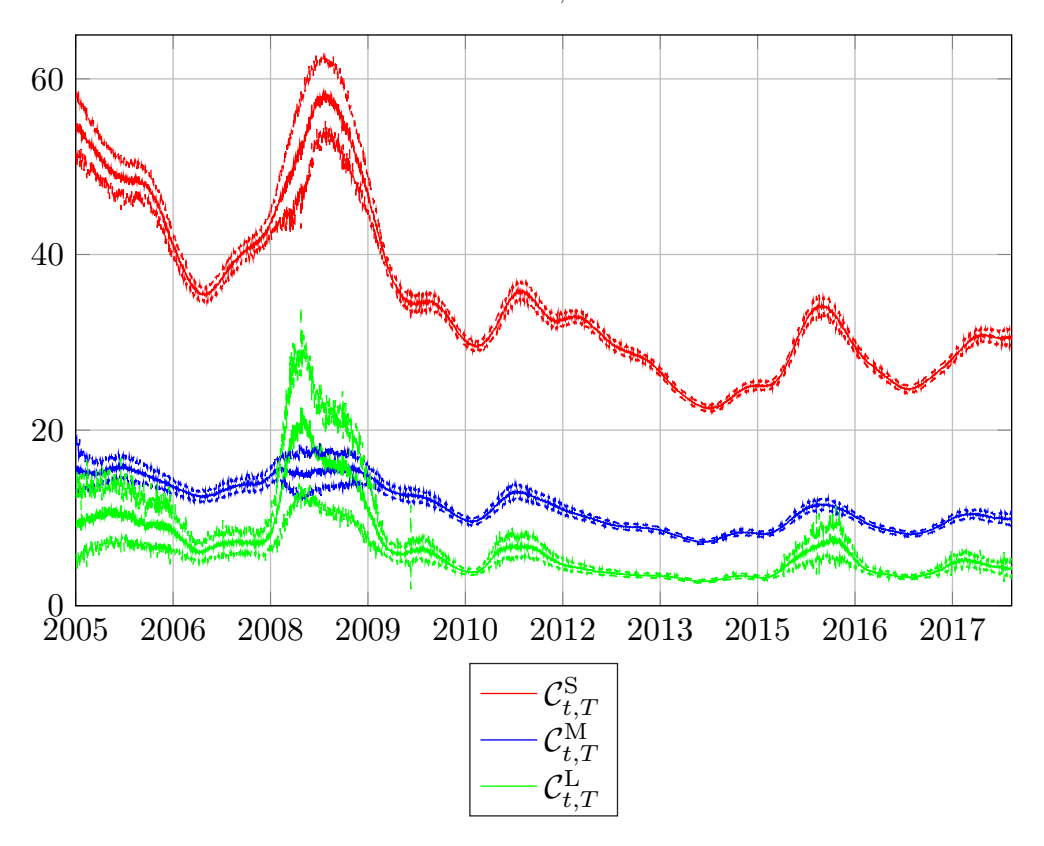


Figure 3: Illiquidity Dynamic Network Connectedness from July 8, 2005 to August 31, 2018 $C_{t,T}^d$, $d = \{S, M, L\}$

This figure plots the quasi posterior median and one standard-deviation percentiles of total illiquidity network connectedness specific to the short-term, medium-term and long-term $\mathcal{C}_{t,T}^d$, $d=\{\mathrm{S},\mathrm{M},\mathrm{L}\}$ for S&P500 stock returns from July 8, 2005 to August 31, 2018. We define short-term, S, as connections made over the 1 day to 1 week horizon; we characterize connections over the medium-term as 1 week to 1-month and long-term as horizons greater than 1 month.

We can see that short-term illiquidity network connectedness is far stronger than medium-term and long-term network connectedness. We expect this to occur since our measures of illiquidity are orthogonal to realized volatility that stem from an OLS regression. Furthermore, observe that peaks in short-term and long-term illiquidity network connectedness appear in conjunction with key stock market events. In particular, connectedness rises: i) during the 2007–2009 recession; ii) late 2010 to mid 2011 that corresponds with the European sovereign debt crisis and bear market in 2011; and iii) the 2015-2016

stock market sell-off where our measures peak in August 2015.

On the whole, our measures provide a useful characterization of illiquidity conditions into their respective horizon specific components. We interpret our measures of illiquidity network connectedness as indexes tracking systemic risk that formulates as a result of illiquidity shock propagation throughout the market. The next section provides two applications that demonstrates the use of our measures in the context of return dynamics and real activity on the basis of theoretical arguments and empirical evidence we outline earlier.

4 Applications of illiquidity network connectedness

In this section, we conduct two exercises that demonstrate the usefulness of our dynamic network measures that from on illiquidity proxies of S&P500 constituents. First, we use total network connectedness and explore the in-sample dynamics with market returns. We then examine the contemporaneous links of total network connectedness with real activity and financial uncertainty indicators.

4.1 Dynamics with the market return

Here we explore the relationship between market returns on total illiquidity connectedness. In doing so, we construct a market capitalisation weighted index using all our S&P500 constituents on a daily basis and use the first order log-difference (multiplied by 100) as the market return, $R_{t,T}$. Within this application our goal is to explore the dynamic relationship between market returns and illiquidity connectedness. This is because studies examining the link between illiquidity and returns suggest that there is a negative link between illiquidity and returns (Chen et al., 2018). Economically this makes sense, as liquidity declines prices fall which causes returns to deplete. In the context of our exercise, as total illiquidity connectedness rises, illiquidity shocks propagate across assets. In turn, liquidity dries up causing prices decline and returns to deteriorate. However, literature also documents: i) time-varying liquidity risk premia; and ii) business cycle contingent predictions of market returns (see e.g. Pástor and Stambaugh, 2003; Watanabe and Watanabe, 2007).

In order to account for the above, we estimate univariate specifications of the timevarying parameter methods in Petrova (2019) of which we provide details in the Appendix C. We control for three popular specifications to obtain loadings; namely the market risk premium; the Fama and French (1993) three factors; and the Fama and French (2015) five factors. All factor data are from Kenneth French's Data Library. In each regression, we include only one of our network connectedness measures which by definition have high correlations. Formally

$$R_{t,T} = \alpha(t/T) + \beta^{\Delta C^d}(t/T)\Delta C_{t-1,T}^d + \beta^{\top}(t/T)\mathbf{X}_{t-1,T} + \epsilon_{t,T} \quad \epsilon_{t,T} \backsim \mathcal{N}\left(0, \sigma_{t,T}^2\right)$$

$$\mathbf{X}_{t-1,T} = \begin{cases} \mathbf{M}\mathbf{K}\mathbf{T}_{t-1,T} \\ \mathbf{M}\mathbf{K}\mathbf{T}_{t-1,T}, \ \mathbf{S}\mathbf{M}\mathbf{B}_{t-1,T}, \ \mathbf{H}\mathbf{M}\mathbf{L}_{t-1,T} \\ \mathbf{M}\mathbf{K}\mathbf{T}_{t-1,T}, \ \mathbf{S}\mathbf{M}\mathbf{B}_{t-1,T}, \ \mathbf{H}\mathbf{M}\mathbf{L}_{t-1,T}, \ \mathbf{C}\mathbf{M}\mathbf{A}_{t-1,T}, \ \mathbf{R}\mathbf{M}\mathbf{W}_{t-1,T} \end{cases}$$

$$(15)$$

where $\alpha(t/T)$ is the time-varying intercept; $\beta^{\Delta C^d}(t/T)$ is the sensitivity of our S&P500 index return to lagged changes in horizon specific or aggregate network connectedness with $d = \{S, M, L, \infty\}$ here ∞ refers to aggregate network connectedness that sums connections over horizons; $\beta^{\top}(t,T)$ is a vector of coefficients holding loadings to other lagged factors we use as controls; and $\mathbf{X}_{t-1,T}$ is a matrix containing lagged factors. $\mathrm{MKT}_{t-1,T}$ is the lagged market risk premium; $\mathrm{SMB}_{t-1,T}$, $\mathrm{HML}_{t-1,T}$, $\mathrm{CMA}_{t-1,T}$, and $\mathrm{RMW}_{t-1,T}$ are the small-minus-big (Fama and French, 1993), high-minus-low (Fama and French, 1993), conservative-minus-aggressive (Fama and French, 2015), and robust-minus-weak (Fama and French, 2015) factors respectively.

Figure 4 reports the beta coefficients associated to changes in aggregate network illiquidity connectedness. In general, it is clear that there is substantial time-variation in the response of market returns to changes in aggregate illiquidity network connectedness. Specifically, we can see that lagged changes result in lower returns from 2007 to 2009 and again in late-2010 and throughout 2011. Returns are most sensitive to changes in aggregate illiquidity network connectedness during 2008 with an economically meaningful (posterior median) estimate hovering around -1.45 in mid-to-late 2008. We also see that during late 2010 and throughout the 2011, the aggregate illiquidity network risk beta becomes significant, both statistically and economically, with a posterior median estimate in the range of -0.4 to -0.5. This period coincides with the European Sovereign debt crisis, the 2010 flash crash, and the S&P500's bear market during spring/summer of 2011.

We now turn to the links between horizon specific network connectedness and the market return. In Figure 5 we plot the betas associated to changes in: i) short-term network connectedness; ii) medium term network connectedness; and iii) long-term network

connectedness. The columns in this figure distinguish between additional controls in each regression. The leftmost columns control for the market risk premium and the middle and rightmost columns control for the Fama and French (1993) 3-factors and Fama and French (2015) 5-factors respectively.

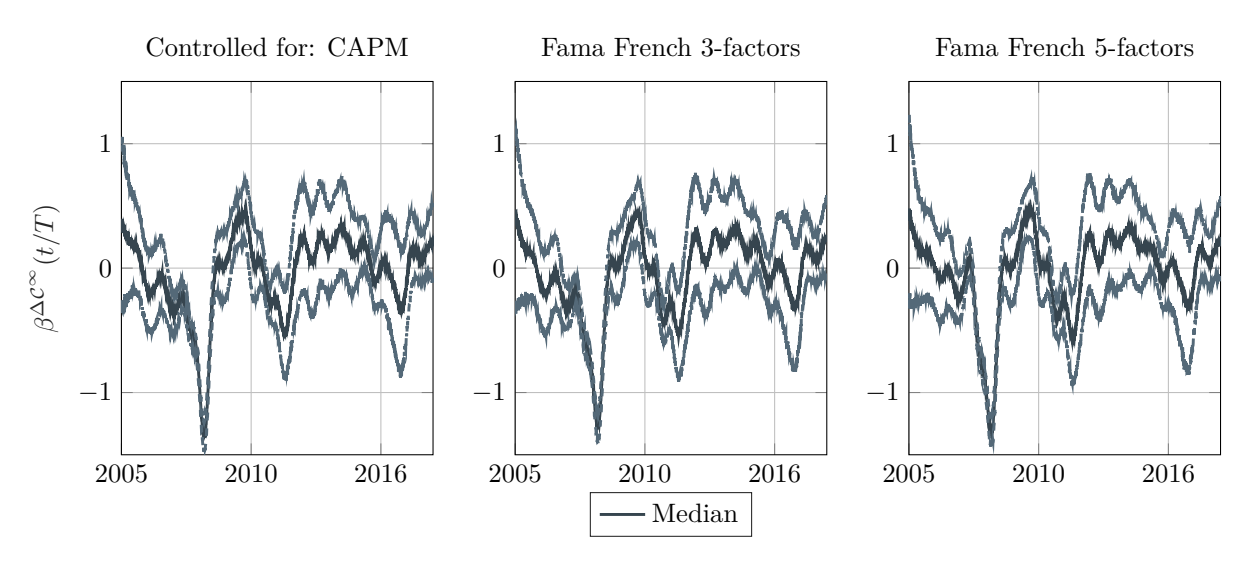


Figure 4: Market return betas with respect to aggregate dynamic network connectedness, $\beta^{\Delta C^{\infty}}(t/T)$

This figure plots the quasi posterior median and one standard-deviation percentiles of beta coefficients with respect to changes in aggregate dynamic network connectedness, $\beta^{\Delta C^{\infty}}(t/T)$, for S&P500 stock returns from July 12, 2005 to August 31, 2018. The leftmost columns are from regressions controlling for the market risk premium, CAPM; the middle columns are from regressions controlling for the Fama and French (1993) 3-factors; and the rightmost columns are from regressions controlling for the Fama and French (2015) 5-factors.

Two main factors emerge from Figure 5. First, the sensitivity of S&P500 returns to changes in horizon specific dynamic network connectedness are robust to controls we account for. In particular, we can see that the time profile of these betas are similar across all specifications. Second, there are substantial differences in the response of market returns to changes in horizon specific dynamic network connectedness. Prior to and during the 2008 recession, S&P500 returns are significantly and positively associated to changes in short-term illiquidity network connectedness. Turning our attention to medium-term and long-term illiquidity network connections during the same period, the impact is negative. The same behaviour occurs in late 2010 and throughout 2011 that corresponds with the European sovereign debt crisis and the short-lived bear market in 2011.

In general, the mechanism between aggregate illiquidity network connectedness and

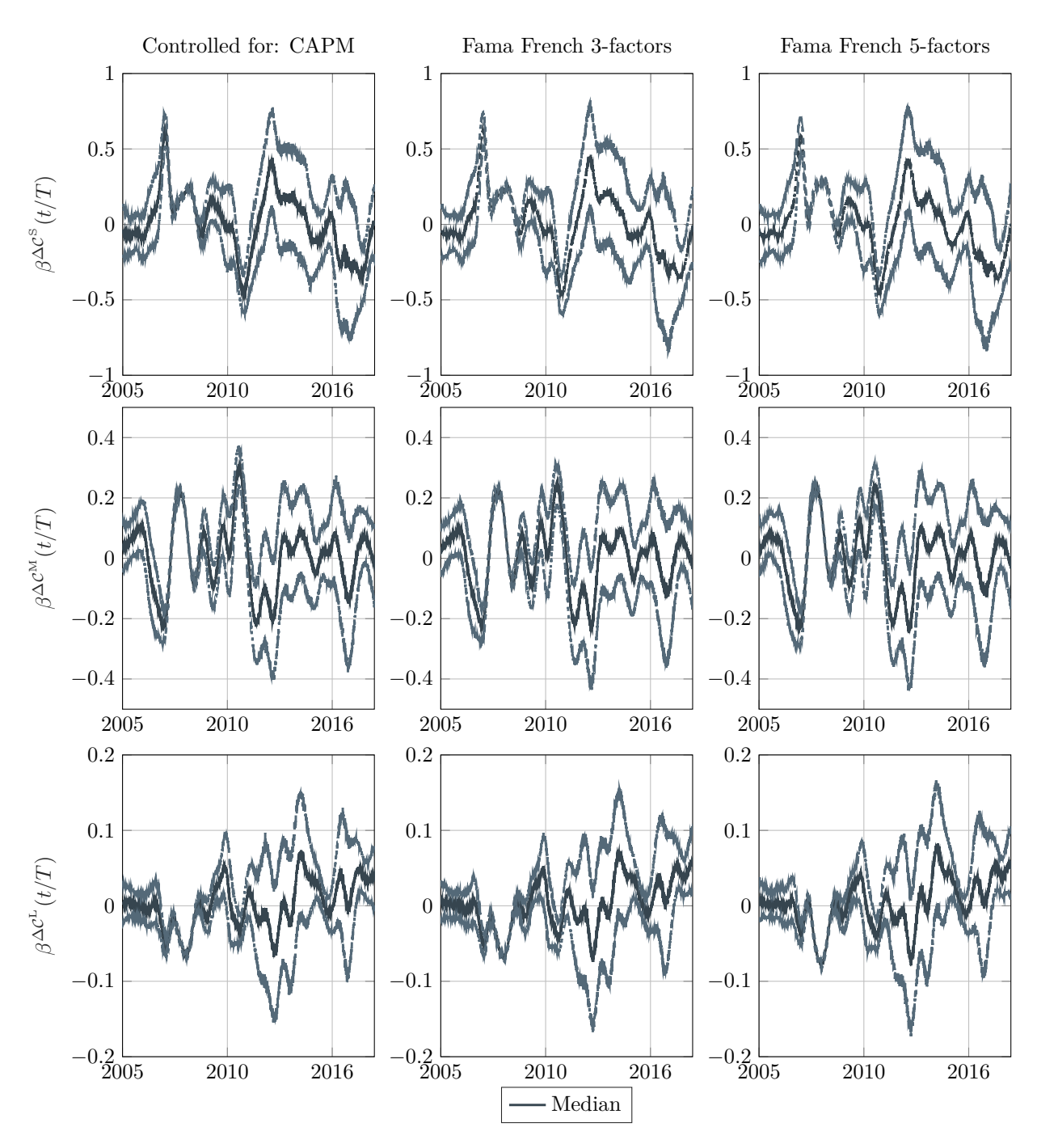


Figure 5: Market return betas with respect to horizon specific dynamic network connectedness, $\beta^{\Delta \mathcal{C}^d}(t/T)$, $d = \{\mathbf{S}, \mathbf{M}, \mathbf{L}\}$

This figure plots the quasi posterior median and one standard-deviation percentiles of beta coefficients with respect to changes in horizon specific dynamic network connectedness, $\beta^{\Delta C^d}(t/T)$, $d=\{S,M,L\}$, for S&P500 stock returns from July 12, 2005 to August 31, 2018. The leftmost columns are from regressions controlling for the market risk premium, CAPM; the middle columns are from regressions controlling for the Fama and French (1993) 3-factors; and the rightmost columns are from regressions controlling for the Fama and French (2015) 5-factors. The top row reports sensitivities of the S&P500 returns to changes in short-term network connectedness, $\beta^{\Delta C}(t/T)$; while the middle and bottom rows show S&P500 return sensitivities to changes in medium-term and long-term network connectedness, $\beta^{\Delta C}(t/T)$, $\beta^{\Delta C}(t/T)$ respectively.

the market return follows the economic intuition; in times of financial turmoil when connections among stocks' illiquidities become increasingly high, the market return becomes more sensitive to these connections and contractions are economically meaningful. We interpret the time-varying sensitivities to aggregate illiquidity connectedness as documenting these "liquidity spirals" in Brunnermeier and Pedersen (2009).

However, we observe opposing effects over short-term network connectedness when comparing to medium-term, and long-term connectedness. We conjecture that the positive impact of short-term network connectedness during the 2008 recession and bear market of 2010-2011 as being attributable to a mispricing phenomenon that is corrected by the respective negative impacts of medium- and long-term network connectedness. Therefore, from an economic perspective we argue that innovations to short-term illiquidity network connectedness can cause puzzling mispricing events for the market, that are lost over the medium to long-run since they have no permanent effect on prices. Nevertheless, this application demonstrates that the network measures we characterize on illiquidity contain useful information investors may wish to use when forming portfolios and/or rebalancing.

4.2 The Information content of illiquidity networks for the real economy and financial uncertainty

Here we examine the information content of illiquidity network connectedness for real activity and financial uncertainty. The financial sector helps the economy function through intermediation. As we outline earlier, a growing literature exists quantifying macrofinancial linkages; particularly through the lens of illiquidity (see e.g. Ellington, 2018). Furthermore, history serves as a reminder that systemic shocks to the financial system can cause deep and long recessions (Hubrich and Tetlow, 2015).

We select the main three monthly indicators that measure economic activity and financial uncertainty, these are: the Aruoba-Diebold-Scotti (ADS) Business Condition Index (Aruoba et al., 2009); the Kansas City Financial Stress Index (KCFSI) (see Hakkio et al., 2009); and the Chicago Board of Exchange (CBOE) VIX. We collect them according to their availability at a monthly frequency⁶. To match the monthly frequency of our

⁶The Aruoba-Diebold-Scotti (ADS) Business Condition Index tracks real business conditions at a high frequency and it is based on economic indicators. It is collected from: https://www.philadelphiafed.org/research-and-data/real-time-center. The Kansas City Financial Stress Index (KCFSI) is a measure of stress in the U.S. financial system based on eleven financial market variables (see Hakkio et al., 2009). It is collected from https://www.kansascityfed.org/research/indicatorsdata/kcfsi.VIX

indicators, we aggregate illiquidity network connectedness measures for a given month and define the monthly illiquidity network connectedness measures as C_t^d , $d = \{S, M, L\}^7$.

Figure 6 reports our real activity and financial uncertainty indicators, along with horizon specific illiquidity network connectedness measures C_t^d , $d = \{S, M, L\}$ on a monthly basis from July 2005 to December 2017. We normalize all variables to have zero mean and unit variance so they are interpretable. The leftmost plot shows the ADS business conditions index. It is clear that our measures of network connectedness have a strong negative link with real activity. Specifically we can see that trough during the 2008 recession corresponds with peaks in our C_t^d , $d = \{S, M, L\}$ measures. Turning to the middle and rightmost plots, there is a clear positive relationship between our measures of illiquidity connectedness and financial uncertainty with peaks and troughs matching throughout these monthly time-series.

For our purposes we want to explore the contemporaneous relationships between our respective measures of illiquidity network connectedness and real activity (financial uncertainty). We therefore focus on first differences of the series we plot in Figure 6. Intuitively, we expect that changes in our illiquidity network connectedness measures have a negative (positive) contemporaneous relationship with changes in real activity (financial uncertainty).

We relate dynamic illiquidity network connectedness using the following OLS regression

$$\Delta X_t = \alpha + \gamma^{\Delta C^d} \Delta C_t^d + \gamma^{\text{ILLIQ}} \Delta \text{ILLIQ}_t^{\text{MKT}} \epsilon_t, \tag{16}$$

where $X_t \in \{\text{ADS}, \text{KCSFI}, \text{VIX}\}$ is one of the macroeconomic and economic uncertainty indicators and $\epsilon_t \sim \text{N}(0, \sigma^2)$. Naturally, we also control for market illiquidity, ILLIQ^{MKT}, that we compute as the Amihud (2002) ratio for individual stocks listed on the NYSE, AMEX and NASDAQ on a daily basis subject to filtering conditions standard in the literature. To compute a market measure, we take the cross sectional average each day and then take the time-series average of daily observations in each month. One can loosely interpret the γ coefficients in Equation 16 as capturing the contemporaneous correlations between real activity (financial uncertainty) and our measures of illiquidity connectedness, after controlling for market illiquidity.

Table 1 reports various specifications of Equation 16 to quantify the contemporanous links between changes in our illiquidity network connectedness measures and real activ-

is the Chicago Board of Exchange implied volatility index collected from Bloomberg.

⁷We drop the double time index here since we aggregate the daily measures to monthly observations and estimate linear OLS regressions in this section.

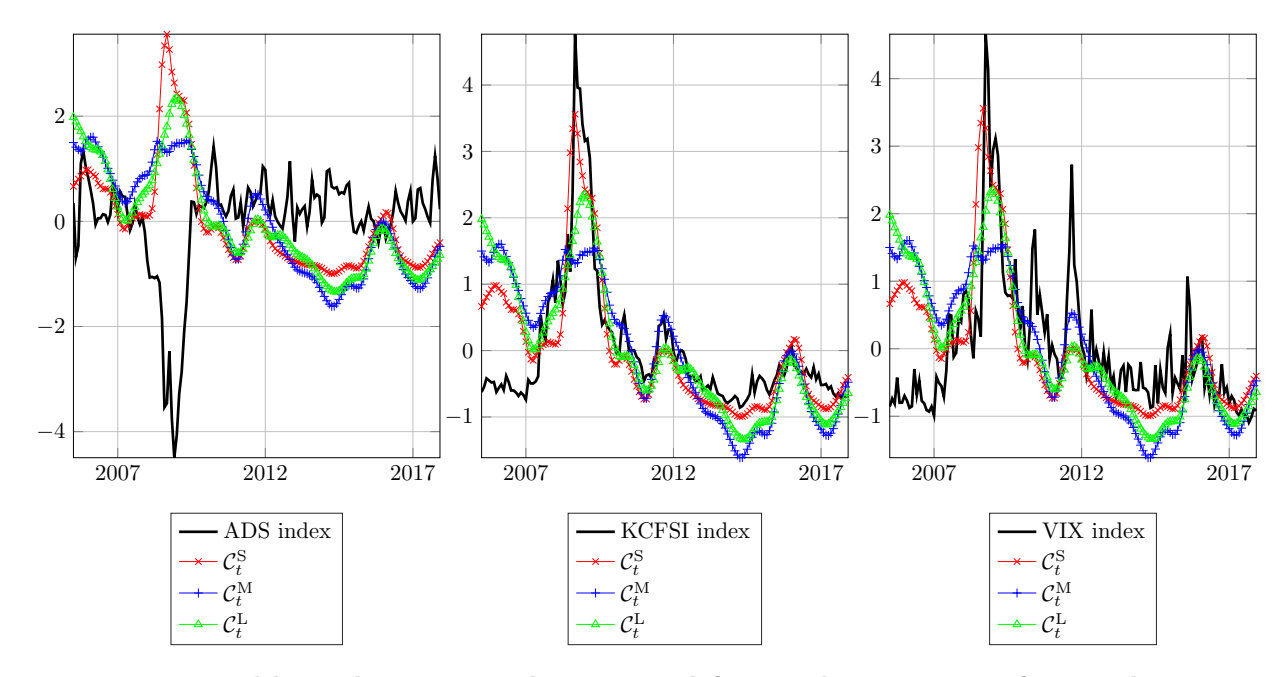


Figure 6: Monthly real activity indicators and financial uncertainty from July 2005 to December 2017

This figure plots real activity and financial uncertainty indicators, along with the quasi posterior median dynamic network connectedness measures at short-term, medium-term and long-term horizons. The leftmost plot shows the Aruoba et al. (2009) (ADS) business conditions index; the middle plot shows the Kansas City Financial Stress Index (KCFSI); and the rightmost plot shows the VIX index. On each plot, we report the horizon specific illiquidity network connectedness measures \mathcal{C}_t^d , $d = \{S, M, L\}$. All variables are standardized to have mean 0 and standard deviation 1 to make the series interpretable.

ity/financial uncertainty. Under each heading, the first specification includes only changes in market illiquidity, the remaining three columns include changes in one of our horizon specific illiquidity network connectedness measures, $\Delta \mathcal{C}_t^d$, $d \in \{S, M, L\}$. Three main factors emerge from these results. First, looking at regressions using ADS (KCFSI/VIX), we can see that all $\gamma^{\Delta \mathcal{C}^d}$, $d \in \{S, M, L\}$ are negative (positive) which is consistent with our expectation. Second, short-term illiquidity connections have a statistically significant contemporaneous link with ADS and KCFSI. Adding to this, the contemporaneous relationship between changes to long-term illiquidity network connectedness and changes to each respective measure of real activity or financial uncertainty are statistically significant. Third, controlling for changes in market illiquidity does not subsume the significance of our network connectedness measures.

Overall, this exercise shows that horizon specific connections among stock illiquidities contain information directly related to real activity and financial uncertainty; particularly over the long-term. Economically speaking, one can interpret our measures as indices for systemic risk that capture horizon specific illiquidity shock propagation. From a theoretical perspective, our results here suggest: i) that our measures better capture the shock propagation mechanism of liquidity shocks in Kiyotaki and Moore (2019); and ii) that the information content of our measures is inherently different to raw measures of stock market illiquidity.

Table 1: Information content of illiquidity network connectedness for real activity and financial uncertainty

Notes: This table reports regression results linking horizon specific illiquidity network connectedness to alternative indicators for economic activity and financial uncertainty. ADS is the Aruoba et al. (2009) business conditions index. KCFSI is the Kansas City Financial Stress Index (Hakkio et al., 2009) and VIX is the CBOE implied volatility index. α is the regression constant; $\gamma^{\Delta C^d}$, $d \in \{S, M, L\}$ are the respective betas associated to short, medium, and long term changes in illiquidity network connectedness; and γ^{ILLIQ} is the coefficient associated to changes in market illiquidity. *, **, and *** denote statistical significance at the 10%, 5% and 1% levels respectively. \bar{R}^2 is the regression adjusted R-squared.

	ADS				KCFSI				VIX			
α	-0.002	-0.004	-0.002	-0.016	0.002	0.008	0.007	0.021	0.022	0.038	0.072	0.195
g	(0.028)	(0.028)	(0.028)	(0.028)	(0.035)	(0.033)	(0.035)	(0.034)	(0.388)	(0.388)	(0.391)	(0.385)
$\gamma^{\Delta \mathcal{C}^{\mathrm{S}}}$		-0.078*				0.207^{***}				0.549		
		(0.042)				(0.050)				(0.586)		
$\gamma^{\Delta \mathcal{C}^{ ext{M}}}$			-0.019				0.147				1.458	
			(0.106)				(0.130)				(1.451)	
$\gamma^{\Delta \mathcal{C}^{ ext{L}}}$				-0.088***				0.120^{***}				1.076^{***}
				(0.029)				(0.036)				(0.405)
$\gamma^{ m ILLIQ}$	-1.450	-1.564	-1.426	-0.441	3.572	3.876*	3.390	2.200	38.905	39.714	37.092	26.549
	(1.870)	(1.856)	(1.881)	(1.852)	(2.310)	(2.195)	(2.314)	(2.273)	(25.743)	(25.769)	(25.806)	(25.653)
\bar{R}^2	-0.003	0.013	-0.009	0.049	0.009	0.107	0.011	0.073	0.009	0.008	0.009	0.048

5 Conclusion

In this paper, we characterize measures of dynamic network connections for large financial and economic systems. Specifically, we assume the market or economy is generated by a TVP VAR model and rely on a locally stationary approximation of the data generating process. Our measures rely on causal linkages by viewing the local forecast error variance decomposition matrices at each point in time as adjacency matrices that completely characterize the dynamic network. We decompose the aggregate dynamic network into components that capture horizon specific connections among systems of financial and economic variables. This allows the researcher or practitioner to study the impact of shock propagation that causes network structures over horizons of interest. In our empirical application we show that our methods are readily available to use in problems using big data. In doing so we redefine the meaning of "big" in big data, in the context of TVP VAR models, and track dynamic connections among illiquidity ratios of all S&P500 constituents.

We then go on to show the usefulness of our dynamic network measures by: i) exploring the dynamic relationship between horizon specific illiquidity network connectedness and the market return and ii) the contemporaneous relation of horizon specific network connections and real activity (financial uncertainty). The former uncovers a strong link between illiquidity connections and the market return that intensifies during periods of financial turbulence. We link this to the self reinforcing mechanism between market and funding liquidity in Brunnermeier and Pedersen (2009) and argue that our measures may be useful for portfolio formation and rebalancing. The latter shows a strong negative (positive) link with real activity (financial stress indicators). We link this with the theoretical mechanism in Kiyotaki and Moore (2019) and conjecture that our illiquidity network connectedness measures are indices that track horizon specific systemic shock propagation.

Acknowledgements

We thank Oliver Linton, Wolfgang Härdle, Catherine Forbes, Lukáš Vácha, Ryland Thomas, Chris Florackis, Costas Milas, Alex Kostakis and Charlie Cai for invaluable discussions and comments. We are grateful to Luboš Hanus for help in furnishing and converting estimation codes. We acknowledge insightful comments from numerous seminar presentations, such as: the 2019 and 2020 Society for Economic Measurement Conferences; the Danish National Bank; the 2019 STAT of ML conference; the 13th International Conference on Computational and Financial Econometrics; and many more. Jozef Baruník gratefully acknowledges support from the Czech Science Founda-

tion under the 19-28231X (EXPRO) project. For estimation of dynamic horizon specific networks, we provide packages DynamicNets.jl in JULIA and DynamicNets in MAT-LAB. The packages are available at https://github.com/barunik/DynamicNets.jl and https://github.com/ellington/DynamicNets.

Disclosure Statement: Jozef Baruník and Michael Ellington have nothing to disclose.

References

- Acemoglu, D., V. M. Carvalho, A. Ozdaglar, and A. Tahbaz-Salehi (2012). The network origins of aggregate fluctuations. *Econometrica* 80(5), 1977–2016.
- Acharya, V. V. and L. H. Pedersen (2005). Asset Pricing with Liquidity Risk. *Journal of Financial Economics* 77(2), 375–410.
- Amihud, Y. (2002). Illiquidity and stock returns: cross-section and time-series effects. Journal of Financial Markets 5(1), 31–56.
- Aruoba, S. B., F. X. Diebold, and C. Scotti (2009). Real-time measurement of business conditions. *Journal of Business & Economic Statistics* 27(4), 417–427.
- Bansal, R., D. Kiku, I. Shaliastovich, and A. Yaron (2014). Volatility, the Macroeconomy, and Asset Prices. *Journal of Finance* 69(6), 2471–2511.
- Baruník, J. and T. Křehlík (2018). Measuring the frequency dynamics of financial connectedness and systemic risk. *Journal of Financial Econometrics* 16(2), 271–296.
- Bekaert, G., C. R. Harvey, and C. Lundblad (2007). Liquidity and Expected Returns: Lessons from Emerging Markets. *Review of Financial Studies* 20(6), 1783–1831.
- Brunnermeier, M. K. and L. H. Pedersen (2009). Market Liquidity and Funding Liquidity. *Review of Financial Studies* 22(6), 2201–2238.
- Chen, Y., G. W. Eaton, and B. S. Paye (2018). Micro (Structure) before Macro? The Predictive Power of Aggregate Illiquidity for Stock Returns and Economic Activity. *Journal of Financial Economics* 130(1), 48–73.
- Chordia, T., R. Roll, and A. Subrahmanyam (2000). Commonality in Liquidity. *Journal* of Financial Economics 56(1), 3–28.

- Dahlhaus, R. (1996). On the kullback-leibler information divergence of locally stationary processes. Stochastic processes and their applications 62(1), 139–168.
- Dahlhaus, R., W. Polonik, et al. (2009). Empirical spectral processes for locally stationary time series. *Bernoulli* 15(1), 1–39.
- Demirer, M., F. X. Diebold, L. Liu, and K. Yilmaz (2018). Estimating global bank network connectedness. *Journal of Applied Econometrics* 33(1), 1–15.
- Diebold, F. X. and K. Yilmaz (2014). On the network topology of variance decompositions: Measuring the connectedness of financial firms. *Journal of Econometrics* 182(1), 119–134.
- Ellington, M. (2018). Financial Market Illiquidity Shocks and Macroeconomic Dynamics: Evidence from the UK. *Journal of Banking & Finance 89*, 225–236.
- Elliott, M., B. Golub, and M. O. Jackson (2014). Financial networks and contagion. *American Economic Review* 104(10), 3115–53.
- Fama, E. F. and K. R. French (1993). Common risk factors in the returns on stocks and bonds. *Journal of Financial Economics* 33(1), 3–56.
- Fama, E. F. and K. R. French (2015). A five-factor asset pricing model. *Journal of Financial Economics* 116(1), 1–22.
- Florackis, C., G. Giorgioni, A. Kostakis, and C. Milas (2014). On Stock Market Illiquidity and Real-time GDP Growth. *Journal of International Money and Finance* 44, 210–229.
- Garvey, M. D., S. Carnovale, and S. Yeniyurt (2015). An analytical framework for supply network risk propagation: A Bayesian network approach. *European Journal of Operational Research* 243(2), 618–627.
- Geraci, M. V. and J.-Y. Gnabo (2018). Measuring interconnectedness between financial institutions with Bayesian time-varying vector autoregressions. *Journal of Financial and Quantitative Analysis* 53(3), 1371–1390.
- Glasserman, P. and H. P. Young (2016). Contagion in financial networks. *Journal of Economic Literature* 54(3), 779–831.
- Goyenko, R. Y., C. W. Holden, and C. A. Trzcinka (2009). Do Liquidity Measures Measure Liquidity? *Journal of Financial Economics* 92(2), 153–181.

- Hakkio, C. S., W. R. Keeton, et al. (2009). Financial stress: what is it, how can it be measured, and why does it matter? *Economic Review* 94(2), 5–50.
- Herskovic, B., B. T. Kelly, H. N. Lustig, and S. Van Nieuwerburgh (2020). Firm volatility in granular networks. *Journal of Political Economy* (Forthcoming).
- Hubrich, K. and R. J. Tetlow (2015). Financial Stress and Economic Dynamics: The Transmission of Crises. *Journal of Monetary Economics* 70, 100–115.
- Kadiyala, K. R. and S. Karlsson (1997). Numerical methods for estimation and inference in Bayesian VAR-models. *Journal of Applied Econometrics* 12(2), 99–132.
- Kiyotaki, N. and J. Moore (2019). Liquidity, business cycles, and monetary policy. *Journal of Political Economy* 127(6), 2926–2966.
- Kyle, A. S. (1985). Continuous Auctions and Insider Trading. Econometrica, 1315–1335.
- Lütkepohl, H. (2005). New introduction to multiple time series analysis. Springer Science & Business Media.
- Næs, R., J. A. Skjeltorp, and B. A. Ødegaard (2011). Stock Market Liquidity and the Business Cycle. *Journal of Finance* 66(1), 139–176.
- Pástor, L. and R. F. Stambaugh (2003). Liquidity risk and expected stock returns. Journal of Political economy 111(3), 642–685.
- Pesaran, H. H. and Y. Shin (1998). Generalized impulse response analysis in linear multivariate models. *Economics letters* 58(1), 17–29.
- Petrova, K. (2019). A quasi-Bayesian local likelihood approach to time varying parameter VAR models. *Journal of Econometrics*.
- Primiceri, G. E. (2005). Time varying structural vector autoregressions and monetary policy. *Review of Economic Studies* 72(3), 821–852.
- Rambachan, A. and N. Shephard (2019). Econometric analysis of potential outcomes time series: instruments, shocks, linearity and the causal response function. arXiv preprint arXiv:1903.01637.
- Richmond, R. J. (2019). Trade network centrality and currency risk premia. *Journal of Finance* 74(3), 1315–1361.

Roueff, F. and A. Sanchez-Perez (2016). Prediction of weakly locally stationary processes by auto-regression. $arXiv\ preprint\ arXiv:1602.01942$.

Watanabe, A. and M. Watanabe (2007). Time-varying Liquidity Risk and the Cross Section of Stock Returns. *Review of Financial Studies* 21(6), 2449–2486.

Technical Appendix

A Proofs: New measures of horizon specific network risk for large dynamic networks

Proposition 1. Let us have the VMA(∞) representation of the locally stationary TVP VAR model (Dahlhaus et al., 2009; Roueff and Sanchez-Perez, 2016)

$$\boldsymbol{X}_{t,T} = \sum_{h=-\infty}^{\infty} \boldsymbol{\Psi}_{t,T}(h) \boldsymbol{\epsilon}_{t-h}$$
(A.1)

 $\Psi_{t,T}(h) \approx \Psi(t/T,h)$ is a stochastic process satisfying $\sup_{\ell} ||\Psi_t - \Psi_{\ell}||^2 = O_p(h/t)$ for $1 \leq h \leq t$ as $t \to \infty$, hence in a neighborhood of a fixed time point u = t/T the process $X_{t,T}$ can be approximated by a stationary process $\widetilde{X}_t(u)$

$$\widetilde{\boldsymbol{X}}_{t}(u) = \sum_{h=-\infty}^{\infty} \boldsymbol{\Psi}(u,h)\boldsymbol{\epsilon}_{t-h}$$
(A.2)

with ϵ being *iid* process with $\mathbb{E}[\epsilon_t] = 0$, $\mathbb{E}[\epsilon_s \epsilon_t] = 0$ for all $s \neq t$, and the local covariance matrix of the errors $\Sigma(u)$. Under suitable regularity conditions $|X_{t,T} - \widetilde{X}_t(u)| = O_p(|t/T - u| + 1/T)$.

Since the errors are assumed to be serially uncorrelated, the total local covariance matrix of the forecast error conditional on the information at time t-1 is given by

$$\Omega(u, H) = \sum_{h=0}^{H} \Psi(u, h) \Sigma(u) \Psi^{\top}(u, h).$$
(A.3)

Next, we consider the local covariance matrix of the forecast error conditional on knowledge of today's shock and future expected shocks to k-th variable. Starting from the conditional forecasting error,

$$\boldsymbol{\xi}^{k}(u,H) = \sum_{h=0}^{H} \boldsymbol{\Psi}(u,h) \left[\boldsymbol{\epsilon}_{t+H-h} - \mathbb{E}(\boldsymbol{\epsilon}_{t+H-h} | \boldsymbol{\epsilon}_{k,t+H-h}) \right], \tag{A.4}$$

assuming normal distribution of $\epsilon_t \sim N(0, \Sigma)$, we obtain⁸

$$\mathbb{E}(\boldsymbol{\epsilon}_{t+H-h}|\boldsymbol{\epsilon}_{k,t+H-h}) = \sigma_{kk}^{-1} \left[\boldsymbol{\Sigma}(u) \right]_{.k} \boldsymbol{\epsilon}_{k,t+H-h}$$
(A.5)

and substituting (A.5) to (A.4), we obtain

$$\boldsymbol{\xi}^{k}(u,H) = \sum_{h=0}^{H} \boldsymbol{\Psi}(u,h) \left[\boldsymbol{\epsilon}_{t+H-h} - \sigma_{kk}^{-1} \left[\boldsymbol{\Sigma}(u) \right]_{\cdot k} \boldsymbol{\epsilon}_{k,t+H-h} \right]. \tag{A.6}$$

Finally, the local forecast error covariance matrix is

$$\mathbf{\Omega}^{k}(u,H) = \sum_{h=0}^{H} \mathbf{\Psi}(u,h) \mathbf{\Sigma}(u) \mathbf{\Psi}^{\top}(u,h) - \sigma_{kk}^{-1} \sum_{h=0}^{H} \mathbf{\Psi}(u,h) \left[\mathbf{\Sigma}(u) \right]_{\cdot k}^{\top} \left[\mathbf{\Sigma}(u) \right]_{\cdot k}^{\top} \mathbf{\Psi}^{\top}(u,h). \tag{A.7}$$

Then

$$\left[\boldsymbol{\Delta}(u,H)\right]_{(j)k} = \left[\boldsymbol{\Omega}(u,H) - \boldsymbol{\Omega}^k(u,H)\right]_{j,j} = \sigma_{kk}^{-1} \sum_{h=0}^{H} \left(\left[\boldsymbol{\Psi}(u,h)\boldsymbol{\Sigma}(u)\right]_{j,k}\right)^2 \tag{A.8}$$

is the unscaled local H-step ahead forecast error variance of the j-th component with respect to the innovation in the k-th component. Scaling the equation with H-step ahead forecast error variance with respect to the jth variable yields the desired time varying generalized forecast error variance decompositions (TVP GFEVD)

$$\left[\boldsymbol{\theta}(u,H)\right]_{j,k} = \frac{\sigma_{kk}^{-1} \sum_{h=0}^{H} \left(\left[\boldsymbol{\Psi}(u,h)\boldsymbol{\Sigma}(u)\right]_{j,k}\right)^{2}}{\sum_{h=0}^{H} \left[\boldsymbol{\Psi}(u,h)\boldsymbol{\Sigma}(u)\boldsymbol{\Psi}^{\top}(u,h)\right]_{j,j}}$$
(A.9)

Next, we derive the frequency representation of the quantity in (A.9) using the fact that unique time varying spectral density of $X_{t,T}$ at frequency ω which is locally the same as the spectral density of $\widetilde{X}_t(u)$ at u = t/T can be defined as a Fourier transform of VMA(∞) filtered series over frequencies $\omega \in (-\pi, \pi)$ as

$$\boldsymbol{S}_{\boldsymbol{X}}(u,\omega) = \sum_{h=-\infty}^{\infty} \mathbb{E}\left[\boldsymbol{X}_{t+h}(u)\boldsymbol{X}_{t}^{\top}(u)\right] e^{-i\omega h} = \left\{\boldsymbol{\Psi}(u)e^{-i\omega}\right\} \boldsymbol{\Sigma}(u) \left\{\boldsymbol{\Psi}(u)e^{+i\omega}\right\}^{\top}, \quad (A.10)$$

⁸Note to notation: $[A]_{j,k}$ denotes the jth row and kth column of matrix A denoted in bold. $[A]_{j,k}$ denotes the full jth row; this is similar for the columns. A $\sum A$, where A is a matrix that denotes the sum of all elements of the matrix A.

where we consider a time varying frequency response function $\Psi(u)e^{-i\omega} = \sum_h e^{-i\omega h}\Psi(u,h)$ which can be obtained as a Fourier transform of the coefficients with $i=\sqrt{-1}$.

Letting $H \to \infty$, we have time varying generalized forecast error variance decompositions

$$\left[\boldsymbol{\theta}(u,\infty)\right]_{j,k} = \frac{\sigma_{kk}^{-1} \sum_{h=0}^{\infty} \left(\left[\boldsymbol{\Psi}(u,h)\boldsymbol{\Sigma}(u)\right]_{j,k}\right)^{2}}{\sum_{h=0}^{\infty} \left[\boldsymbol{\Psi}(u,h)\boldsymbol{\Sigma}(u)\boldsymbol{\Psi}^{\top}(u,h)\right]_{j,j}} = \frac{\mathcal{A}}{\mathcal{B}}.$$
(A.11)

Starting with frequency domain counterpart of the nominator \mathcal{A} , we will use the standard integral

$$\frac{1}{2\pi} \int_{-\pi}^{\pi} e^{i\omega(r-v)} d\omega = \begin{cases} 1 & \text{for } r=v \\ 0 & \text{for } r \neq v. \end{cases}$$
 (A.12)

Using the fact that $\sum_{h=0}^{\infty} \phi(h)\psi(h) = \frac{1}{2\pi} \int_{-\pi}^{\pi} \sum_{v=0}^{\infty} \sum_{r=0}^{\infty} \phi(r)\psi(v)e^{i\omega(r-v)}d\omega$, we can rewrite (A.11) as

$$\begin{split} \sigma_{kk}^{-1} \sum_{h=0}^{\infty} & \left(\left[\mathbf{\Psi}(u,h) \mathbf{\Sigma}(u) \right]_{j,k} \right)^{2} = \sigma_{kk}^{-1} \sum_{h=0}^{\infty} \left(\sum_{z=1}^{n} \left[\mathbf{\Psi}(u,h) \right]_{j,z} \left[\mathbf{\Sigma}(u) \right]_{z,k} \right)^{2} \\ & = \sigma_{kk}^{-1} \frac{1}{2\pi} \int_{-\pi}^{\pi} \sum_{r=0}^{\infty} \sum_{v=0}^{\infty} \left(\sum_{x=1}^{n} \left[\mathbf{\Psi}(u,r) \right]_{j,x} \left[\mathbf{\Sigma}(u) \right]_{x,k} \right) \left(\sum_{y=1}^{n} \left[\mathbf{\Psi}(u,v) \right]_{j,y} \left[\mathbf{\Sigma}(u) \right]_{y,k} \right) e^{i\omega(r-v)} d\omega \\ & = \sigma_{kk}^{-1} \frac{1}{2\pi} \int_{-\pi}^{\pi} \sum_{r=0}^{\infty} \sum_{v=0}^{\infty} \left(\sum_{x=1}^{n} \left[\mathbf{\Psi}(u,r) e^{i\omega r} \right]_{j,x} \left[\mathbf{\Sigma}(u) \right]_{x,k} \right) \left(\sum_{y=1}^{n} \left[\mathbf{\Psi}(u,v) e^{-i\omega v} \right]_{j,y} \left[\mathbf{\Sigma}(u) \right]_{y,k} \right) d\omega \\ & = \sigma_{kk}^{-1} \frac{1}{2\pi} \int_{-\pi}^{\pi} \left(\sum_{x=1}^{n} \left[\mathbf{\Psi}(u) e^{i\omega} \right]_{j,x} \left[\mathbf{\Sigma}(u) \right]_{x,k} \right) \left(\sum_{y=1}^{n} \left[\mathbf{\Psi}(u) e^{-i\omega} \right]_{j,y} \left[\mathbf{\Sigma}(u) \right]_{y,k} \right) d\omega \\ & = \sigma_{kk}^{-1} \frac{1}{2\pi} \int_{-\pi}^{\pi} \left(\left[\mathbf{\Psi}(u) e^{-i\omega} \mathbf{\Sigma}(u) \right]_{j,k} \right) \left(\left(\mathbf{\Psi}(u) e^{i\omega} \mathbf{\Sigma}(u) \right]_{j,k} \right) d\omega \\ & = \sigma_{kk}^{-1} \frac{1}{2\pi} \int_{-\pi}^{\pi} \left[\left[\mathbf{\Psi}(u) e^{-i\omega} \mathbf{\Sigma}(u) \right]_{j,k} \right] d\omega \end{aligned}$$

$$(A.13)$$

Hence we have established that

$$\mathcal{A} = \sigma_{kk}^{-1} \sum_{h=0}^{\infty} \left(\left[\mathbf{\Psi}(u,h) \mathbf{\Sigma}(u) \right]_{j,k} \right)^2 = \sigma_{kk}^{-1} \frac{1}{2\pi} \int_{-\pi}^{\pi} \left| \left[\mathbf{\Psi}(u) e^{-i\omega} \mathbf{\Sigma}(u) \right]_{j,k} \right|^2 d\omega$$
 (A.14)

from (A.11), we use the local spectral representation of the VMA coefficients in the second step. The rest is a manipulation with the last step invoking the definition of modulus squared of a complex number to be defined as $|z|^2 = zz^*$. Note that we can use this simplification without loss of generality, because the $VMA(\infty)$ representation that is described by the coefficients $\Psi(u,h)$ has a spectrum that is always symmetric.

Next, we concentrate on \mathcal{B} from (A.11). Using similar steps and the positive semidefiniteness of the matrix $\Sigma(u)$ that ascertains that there exists P(u) such that $\Sigma(u) = P(u)P^{\top}(u)$.

$$\sum_{h=0}^{\infty} \left[\mathbf{\Psi}(u,h) \mathbf{\Sigma}(u) \mathbf{\Psi}^{\top}(u,h) \right] = \sum_{h=0}^{\infty} \left[\mathbf{\Psi}(u,h) \mathbf{P}(u) \right] \left[\mathbf{\Psi}(u,h) \mathbf{P}(u) \right]^{\top} \\
= \frac{1}{2\pi} \int_{-\pi}^{\pi} \sum_{r=0}^{\infty} \sum_{v=0}^{\infty} \left[\mathbf{\Psi}(u,r) e^{i\omega r} \mathbf{P}(u) \right] \left[\mathbf{\Psi}(u,v) e^{-i\omega v} \mathbf{P}(u) \right]^{\top} d\omega \\
= \frac{1}{2\pi} \int_{-\pi}^{\pi} \sum_{r=0}^{\infty} \left[\mathbf{\Psi}(u,r) e^{i\omega r} \mathbf{P}(u) \right] \sum_{v=0}^{\infty} \left[\mathbf{\Psi}(u,v) e^{-i\omega v} \mathbf{P}(u) \right]^{\top} d\omega \\
= \frac{1}{2\pi} \int_{-\pi}^{\pi} \left[\mathbf{\Psi}(u) e^{i\omega} \mathbf{P}(u) \right] \left[\mathbf{\Psi}(u) e^{-i\omega} \mathbf{P}(u) \right]^{\top} d\omega \\
= \frac{1}{2\pi} \int_{-\pi}^{\pi} \left[\left\{ \mathbf{\Psi}(u) e^{i\omega} \right\} \mathbf{\Sigma}(u) \left\{ \mathbf{\Psi}(u) e^{-i\omega} \right\}^{\top} \right] d\omega \tag{A.15}$$

That establishes the fact that

$$\mathcal{B} = \sum_{h=0}^{\infty} \left[\mathbf{\Psi}(u,h) \mathbf{\Sigma}(u) \mathbf{\Psi}^{\top}(u,h) \right]_{j,j} = \frac{1}{2\pi} \int_{-\pi}^{\pi} \left[\left\{ \mathbf{\Psi}(u) e^{i\omega} \right\} \mathbf{\Sigma}(u) \left\{ \mathbf{\Psi}(u) e^{-i\omega} \right\}^{\top} \right]_{j,j} d\omega \quad (A.16)$$

from (A.11), and we have shown that

$$\left[\boldsymbol{\theta}(u,\infty)\right]_{j,k} = \frac{\sigma_{kk}^{-1} \sum_{h=0}^{\infty} \left(\left[\boldsymbol{\Psi}(u,h)\boldsymbol{\Sigma}(u)\right]_{j,k}\right)^{2}}{\sum_{h=0}^{\infty} \left[\boldsymbol{\Psi}(u,h)\boldsymbol{\Sigma}(u)\boldsymbol{\Psi}^{\top}(u,h)\right]_{j,j}} = \frac{\sigma_{kk}^{-1} \int_{-\pi}^{\pi} \left[\left[\boldsymbol{\Psi}(u)e^{-i\omega}\boldsymbol{\Sigma}(u)\right]_{j,k}\right]^{2} d\omega}{\int_{-\pi}^{\pi} \left[\left\{\boldsymbol{\Psi}(u)e^{i\omega}\right\}\boldsymbol{\Sigma}(u)\left\{\boldsymbol{\Psi}(u)e^{-i\omega}\right\}^{\top}\right]_{j,j} d\omega}$$
(A.17)

Finally, focusing on a frequency band $d = (a, b) : a, b \in (-\pi, \pi), a < b$, we have

$$\left[\boldsymbol{\theta}(u,d)\right]_{j,k} = \frac{\sigma_{kk}^{-1} \int_{a}^{b} \left[\left[\boldsymbol{\Psi}(u)e^{-i\omega}\boldsymbol{\Sigma}(u)\right]_{j,k}\right]^{2} d\omega}{\int_{-\pi}^{\pi} \left[\left\{\boldsymbol{\Psi}(u)e^{i\omega}\right\}\boldsymbol{\Sigma}(u)\left\{\boldsymbol{\Psi}(u)e^{-i\omega}\right\}^{\top}\right]_{j,j} d\omega}$$
(A.18)

This completes the proof.

Proposition 2. Using the Remark 1 and appropriate substitutions, it immediately follows that

$$\sum_{d_{s}\in D} \mathcal{C}(u, d_{s}) = \sum_{d_{z}\in D} \left(\sum_{\substack{j,k=1\\j\neq k}}^{N} \left[\widetilde{\boldsymbol{\theta}}(u, d_{s}) \right]_{j,k} \middle/ \sum_{\substack{j,k=1\\j\neq k}}^{N} \left[\widetilde{\boldsymbol{\theta}}(u, \infty) \right]_{j,k} \right)$$

$$= \left(\sum_{d_{z}\in D} \sum_{\substack{j,k=1\\j\neq k}}^{N} \left[\widetilde{\boldsymbol{\theta}}(u, d_{s}) \right]_{j,k} \middle/ \sum_{\substack{j,k=1\\j\neq k}}^{N} \left[\widetilde{\boldsymbol{\theta}}(u, \infty) \right]_{j,k} \middle/ \sum_{j,k=1}^{N} \left[\widetilde{\boldsymbol{\theta}}(u, \infty) \right]_{j,k} \right)$$

$$= \sum_{j,k=1}^{N} \left[\widetilde{\boldsymbol{\theta}}(u, \infty) \right]_{j,k} \middle/ \sum_{j,k=1}^{N} \left[\widetilde{\boldsymbol{\theta}}(u, \infty) \right]_{j,k}$$

$$= \mathcal{C}(u, \infty)$$
(A.19)

Similarly, quantities $C_{j\leftarrow \bullet}(u,\infty)$ and $C_{j\rightarrow \bullet}(u,\infty)$ will sum over frequency bands. This completes the proof.

B Estimation of the time-varying parameter VAR model

To estimate our high dimensional systems, we follow the Quasi-Bayesian Local-Liklihood (QBLL) approach of Petrova (2019). let X_t be an $N \times 1$ vector generated by a stable time-varying parameter (TVP) heteroskedastic VAR model with p lags:

$$\boldsymbol{X}_{t,T} = \boldsymbol{\Phi}_1(t/T)\boldsymbol{X}_{t-1,T} + \ldots + \boldsymbol{\Phi}_p(t/T)\boldsymbol{X}_{t-p,T} + \boldsymbol{\epsilon}_{t,T}, \tag{B.1}$$

where $\boldsymbol{\epsilon}_{t,T} = \boldsymbol{\Sigma}^{-1/2}(t/T)\boldsymbol{\eta}_{t,T}$ with $\boldsymbol{\eta}_{t,T} \sim NID(0, \boldsymbol{I}_M)$ and $\boldsymbol{\Phi}(t/T) = (\boldsymbol{\Phi}_1(t/T), \dots, \boldsymbol{\Phi}_p(t/T))^{\top}$ are the time varying autoregressive coefficients. Note that all roots of the locally stationary VAR polynomial, lie outside the unit circle, and $\boldsymbol{\Sigma}_t^{-1}$ is a positive definite time-varying covariance matrix. Stacking the time-varying intercepts and autoregressive matrices in the vector $\boldsymbol{\phi}(t/T)$ with $\boldsymbol{X}_{t,T}' = (\boldsymbol{I}_N \otimes x_{t,T})$, $x_{t,T} = (1, x'_{t-1,T}, \dots, x'_{t-p,T})$ and $\boldsymbol{\omega}$ denotes the Kronecker product, the model can be written as:

$$\boldsymbol{X}_{t,T} = \bar{\boldsymbol{X}}'_{t,T}\phi(t/T) + \boldsymbol{\Sigma}^{-\frac{1}{2}}(t/T)\boldsymbol{\eta}_{t,T}$$
(B.2)

We obtain the time-varying parameters of the model by employing Quasi-Bayesian Local Likelihood (QBLL) methods. Estimation of (B.1) requires re-weighting the likelihood function. Essentially, the weighting function gives higher proportions to observations surrounding the time period whose parameter values are of interest. The local likelihood function at discrete time period s, where we drop the double time index for notational convenience, is given by:

$$L_{s}\left(\boldsymbol{X}_{s}|\phi_{s},\boldsymbol{\Sigma}_{s},\bar{\boldsymbol{X}}_{s}\right) \propto |\boldsymbol{\Sigma}_{s}|^{\operatorname{trace}(\boldsymbol{\mathbf{D}}_{s})/2} \exp\left\{-\frac{1}{2}(\boldsymbol{X}_{s}-\bar{\boldsymbol{X}}_{s}'\phi_{s})'(\boldsymbol{\Sigma}_{s}\otimes\boldsymbol{\mathbf{D}}_{s})(\boldsymbol{X}_{s}-\bar{\boldsymbol{X}}_{s}'\phi_{s})\right\}$$
(B.3)

The \mathbf{D}_s is a diagonal matrix whose elements hold the weights:

$$\mathbf{D}_s = \operatorname{diag}(\varrho_{s1}, \dots, \varrho_{sT}) \tag{B.4}$$

$$\varrho_{st} = \zeta_{T,s} w_{st} / \sum_{t=1}^{T} w_{st} \tag{B.5}$$

$$w_{st} = (1/\sqrt{2\pi}) \exp((-1/2)((k-t)/H)^2), \text{ for } s, t \in \{1, \dots, T\}$$
 (B.6)

$$\zeta_{Ts} = \left(\left(\sum_{t=1}^{T} w_{st} \right)^2 \right)^{-1} \tag{B.7}$$

where ϱ_{st} is a normalised kernel function. w_{st} uses a Normal kernel weighting function. ζ_{Ts} gives the rate of convergence and behaves like the bandwidth parameter H in (B.6), and it is the kernel function that provides greater weight to observations surrounding the parameter estimates at time s relative to more distant observations.

Using a Normal-Wishart prior distribution for $\phi_s | \Sigma_s$ for $s \in \{1, \dots, T\}$:

$$\phi_s | \Sigma_s \backsim \mathcal{N} \left(\phi_{0s}, (\Sigma_s \otimes \Xi_{0s})^{-1} \right)$$
 (B.8)

$$\Sigma_s \backsim \mathcal{W}(\alpha_{0s}, \Gamma_{0s})$$
 (B.9)

where ϕ_{0s} is a vector of prior means, Ξ_{0s} is a positive definite matrix, α_{0s} is a scale parameter of the Wishart distribution (W), and Γ_{0s} is a positive definite matrix.

The prior and weighted likelihood function implies a Normal-Wishart quasi posterior distribution for $\phi_s | \Sigma_s$ for $s = \{1, \ldots, T\}$. Formally let $\mathbf{A} = (\bar{x}_1', \ldots, \bar{x}_T')'$ and $\mathbf{Y} = (x_1, \ldots, x_T)'$ then:

$$\phi_s | \mathbf{\Sigma}_s, \mathbf{A}, \mathbf{Y} \sim \mathcal{N}\left(\tilde{\phi}_s, \left(\mathbf{\Sigma}_s \otimes \tilde{\mathbf{\Xi}}_s\right)^{-1}\right)$$
 (B.10)

$$\Sigma_s \backsim \mathcal{W}\left(\tilde{\alpha}_s, \tilde{\Gamma}_s^{-1}\right)$$
 (B.11)

with quasi posterior parameters

$$\tilde{\phi}_s = \left(\mathbf{I}_N \otimes \tilde{\mathbf{\Xi}}_s^{-1}\right) \left[\left(\mathbf{I}_N \otimes \mathbf{A}' \mathbf{D}_s \mathbf{A}\right) \hat{\phi}_s + \left(\mathbf{I}_N \otimes \mathbf{\Xi}_{0s}\right) \phi_{0s} \right]$$
(B.12)

$$\tilde{\mathbf{\Xi}}_{s} = \tilde{\mathbf{\Xi}}_{0s} + \mathbf{A}' \mathbf{D}_{s} \mathbf{A} \tag{B.13}$$

$$\tilde{\alpha}_s = \alpha_{0s} + \sum_{t=1}^T \varrho_{st} \tag{B.14}$$

$$\tilde{\mathbf{\Gamma}}_{s} = \mathbf{\Gamma}_{0s} + \mathbf{Y}' \mathbf{D}_{s} \mathbf{Y} + \mathbf{\Phi}_{0s} \mathbf{\Gamma}_{0s} \mathbf{\Phi}'_{0s} - \tilde{\mathbf{\Phi}}_{s} \tilde{\mathbf{\Gamma}}_{s} \tilde{\mathbf{\Phi}}'_{s}$$
(B.15)

where $\hat{\phi}_s = (\mathbf{I}_N \otimes \mathbf{A}' \mathbf{D}_s \mathbf{A})^{-1} (\mathbf{I}_N \otimes \mathbf{A}' \mathbf{D}_s) y$ is the local likelihood estimator for ϕ_s . The matrices Φ_{0s} , $\tilde{\Phi}_s$ are conformable matrices from the vector of prior means, ϕ_{0s} , and a draw from the quasi posterior distribution, $\tilde{\phi}_s$, respectively.

The motivation for employing these methods are threefold. First, we are able to estimate large systems that conventional Bayesian estimation methods do not permit. This is typically because the state-space representation of an N-dimensional TVP VAR (p) requires an additional N(3/2 + N(p + 1/2)) state equations for every additional variable. Conventional Markov Chain Monte Carlo (MCMC) methods fail to estimate larger models, which in general confine one to (usually) fewer than 6 variables in the system. Second, the standard approach is fully parametric and requires a law of motion. This can distort inference if the true law of motion is misspecified. Third, the methods used here permit direct estimation of the VAR's time-varying covariance matrix, which has an inverse-Wishart density and is symmetric positive definite at every point in time.

In estimating the model, we use p=2 and a Minnesota Normal-Wishart prior with a shrinkage value $\varphi=0.05$ and centre the coefficient on the first lag of each variable to 0.1 in each respective equation. The prior for the Wishart parameters are set following Kadiyala and Karlsson (1997). For each point in time, we run 500 simulations of the model to generate the (quasi) posterior distribution of parameter estimates. Note we experiment with various lag lengths, $p=\{2,3,4,5\}$; shrinkage values, $\varphi=\{0.01,0.25,0.5\}$; and values to centre the coefficient on the first lag of each variable, $\{0,0.05,0.2,0.5\}$. Network measures from these experiments are qualitatively similar. Notably, adding lags to the VAR and increasing the persistence in the prior value of the first lagged dependent variable in each equation increases computation time.

C Univariate time-varying parameter regressions

We now consider a linear regression with time-varying parameters that has a Normal-Gamma quasi-posterior distribution. Specifically, this is a univariate version of Petrova (2019). Let

$$y_{t,T} = \beta_0(t/T) + x_{1,t,T}\beta_1(t/T) + \dots + x_{l,t,T}\beta_l(t/T) + \epsilon_{t,T}, \quad \epsilon_{t,T} \backsim \mathcal{N}\left(0, \sigma_{t,T}^2\right) (\text{C}.1)$$

$$y_{t,T} = x_{t,T}\beta(t/T) + \epsilon_{t,T} \tag{C}.2$$

where $x_{t,T} \equiv (1, x_{1,t,T}, \dots, x_{l,t,T})$ and $\beta(t/T) \equiv (\beta_0(t/T), \beta_1(t/T), \dots, \beta_l(t/T))^{\top}$. Now let $\lambda_{t,T} \equiv \sigma_{t,T}^{-2}$. The weighted local likelihood function of the sample $Y \equiv$ (y_1, \ldots, y_T) , using $\mathbf{X} \equiv (x_1^\top, \ldots, x_T^\top)^\top$ as a $T \times l$ matrix, at each discrete time point s, where we drop the double time index for notational convenience, is given by

$$L_s(Y|\beta_s, \lambda_s, \mathbf{X}) =$$

$$(2\pi)^{-\operatorname{tr}(\mathbf{D}_s)/2} \lambda_s^{\operatorname{tr}(\mathbf{D}_s)/2} \exp\left\{-\frac{\lambda_s}{2} (Y - \mathbf{X}\beta_s)^{\top} \mathbf{D}_s (Y - \mathbf{X}\beta_s)\right\} \quad (C.3)$$

with

$$\mathbf{D}_{s} = \operatorname{diag}(\vartheta_{s,1}, \dots, \vartheta_{s,T}) \tag{C.4}$$

$$\vartheta_{s,t} = \zeta_{T,s} w_{s,t} / \sum_{t=1}^{T} w_{s,t}$$
 (C.5)

$$w_{s,t} = (1/\sqrt{2\pi}) \exp((-1/2)((k-t)/H)^2), \forall s, t \in \{1, \dots, T\}$$
 (C.6)

$$\zeta_{T,s} = \left(\sum_{t=1}^{T} w_{s,t}^{2}\right)^{-1}$$
(C.7)

Now assuming β_s , λ_s have a Normal-Gamma prior distribution $\forall s \in \{1, \dots, T\}$

$$\beta_s | \lambda_s \sim \mathcal{N} \left(\beta_{0,s}, (\lambda_s \kappa_{0,s})^{-1} \right)$$
 (C.8)

$$\lambda_s \sim \mathcal{G}(\alpha_{0,s}, \gamma_{0,s})$$
 (C.9)

We can combine L_s with the above priors such that β_s , λ_s have Normal-Gamma quasi-posterior distribution $\forall k \in \{1, ..., T\}$

$$\beta_s | \lambda_s \sim \mathcal{N}\left(\bar{\beta}_s, (\lambda_s \bar{\kappa}_s)^{-1}\right)$$
 (C.10)

$$\lambda_s \backsim \mathcal{G}(\bar{\alpha}_s, \bar{\gamma}_s)$$
 (C.11)

with (quasi) posterior parameters:

$$\bar{\beta}_s = \bar{\kappa}_s^{-1} \left(\mathbf{X}^\top \mathbf{D}_s \mathbf{X} \hat{\beta}_s + \kappa_{0,s} \beta_{0,s} \right), \ \hat{\beta}_s = \left(\mathbf{X}^\top \mathbf{D}_s \mathbf{X} \right)^{-1} \mathbf{X}^\top \mathbf{D}_s y$$
 (C.12)

$$\bar{\kappa}_s = \kappa_{0,s} + \mathbf{X}^{\mathsf{T}} \mathbf{D}_s \mathbf{X} \tag{C.13}$$

$$\bar{\alpha}_s = \alpha_{0,s} + \sum_{t=1}^T \vartheta_s \tag{C.14}$$

$$\bar{\gamma}_s = \gamma_{0,s} + \frac{1}{2} \left(Y^\top \mathbf{D}_s Y - \bar{\beta}_s^\top \bar{\kappa}_s \bar{\beta}_s + \beta_{0,s}^\top \kappa_{0,s} \beta_{0,s} \right)$$
 (C.15)

The Algorithm

- 1. Initialise $\beta_{0,s}$, $\kappa_{0,s}$, $\alpha_{0,s}$, $\gamma_{0,s}$ and compute kernel weights. Then repeat steps 2-3 $\iota = 1, 2, \ldots, \mathcal{I}$ times.
- 2. For every $s \in \{1, 2, ..., T\}$, draw $\lambda_s^s | \mathbf{X}, y, \beta_s^{s-1}$ from $\backsim \mathcal{G}(\bar{\alpha}_s, \bar{\gamma}_s)$.
- 3. For every $s \in \{1, 2, \dots, T\}$, draw $\beta_s^s | y, \mathbf{X}, \lambda_s^s$ from $\backsim \mathcal{N}\left(\bar{\beta}_s, (\lambda_s \bar{\kappa}_s)^{-1}\right)$.

In our case, for each regression in Section 4.1 we set the parameter $H = \sqrt{T}$ to compute the kernel weights and initialize $\beta_{0,s}$, $\kappa_{0,s}$, $\alpha_{0,s}$, $\gamma_{0,s}$ using OLS parameters from a linear regression for the time-series in question. Then, we generate $\mathcal{I}=1000$ simulations for each time-period. The estimations are carried out using parallel computing on a desktop machine with 64GB of RAM, an Intel 3.70GHz i7-8700K processor with 6-cores. Note we also estimate regressions containing only changes in illiquidity network connectedness individually. Results do not change qualitatively and are available on request. The total estimation time for 16 models, 12 models we present in the main text plus the 4 models for extra robustness purposes, is 1496 seconds.